Single-cell screening of molecular phenotypes using droplet-based microfluidics

Michael Schubert

13th February 2013

MSc Thesis

Institute for Molecular Biotechnology

Graz University of Technology

Austria

TUG Supervisor: Prof. Helmut Schwab

External Supervisors: Dr. Christoph Merten and Dr. Jan Korbel

European Molecular Biology Laboratory (EMBL) Heidelberg

Germany

Abstract

Cancer is a heterogeneous disease, given rise by the malignant transformation of cells that in turn gain the ability to proliferate to a point that is detrimental to the organism they reside in. It has claimed many lives, second only to cardiovascular diseases in wealthy countries. Most patients with cancer die not because of the primary tumour, but the dissemination of individual tumour cells that colonise distant sites to form metastases. Cancer cells need to attain a specific set of traits that enables them to proliferate, maintain a microenvironment that aids them in their cause, and subsequently use the bloodstream as a vector to colonise foreign tissue.

Matrix metalloproteinases (MMPs) play a crucial role in both physiological processes and cancer pathology. While in both cases they regulate apoptosis, remodel tissue and vasculature, and modulate immune function, in the latter they also act in the process of tissue degradation by cleaving compounds of the extracellular matrix. However, not all cells in a tumour are cancerous and only some secrete MMPs, along with other cells of the microenvironment. It is our goal to obtain populations of cancer cells that do and do not secrete MMPs, and determine the genetic differences between them.

In this work, droplet-based microfluidics was used to encapsulate single cells in aequous microcompartments, or droplets, along with a FRET peptide to assay their MMP activity and sort positive droplets by dielectrophoresis afterwards, allowing whole genome sequencing of the recovered cellular contents from both the positive and the negative subpopulation. The assay was established using the HeLa and HT-1080 cell lines, where the latter was known to express these enzymes on the cells' surface and used to probe primary prostate tumour cells for their expression patterns. Identifying the genetic determinants that give rise to the secretion of these enzymes could lead to targets for drug development later on.

Zusammenfassung

Krebs ist eine heterogene Erkrankung, die dadurch entsteht, dass körpereigene Zellen eine maligne Transformation untergehen und sich dadurch unkontrolliert vermehren. Die Krankheit selbst verursacht die zweitmeisten Todesfälle in der westlichen Welt, übertroffen nur von Herz-Kreislauferkrankungen. Die meisten Patienten für die die Krankheit fatal endet sterben nicht an dem primären Tumor, sondern an Metastasen, die einzelne Krebszellen in fremden Geweben begründen, nachdem sie gewisse Eigenschaften erworben haben, sich vom primären Tumor lösen, und über den Blutkreislauf zu anderen Standorten wandern.

Matrix Metalloproteinasen (MMPs) spielen dabei eine bedeutende Rolle, wie auch in physiologischen Prozessen. In beiden Fällen regulieren sie Apoptose, die Umstrukturierung von Geweben und die Immunfunktion, und im Fall von Krebsentwicklung auch den Abbau der extrazellulären Matrix zur Gewebsinvasion. Jedoch sezernieren nicht alle Krebszellen MMPs und nicht alle Zellen die MMPs sezernieren sind Krebszellen. Ziel dieses Projekts ist es, die genetischen Unterschiede zwischen Krebszellen die MMPs sezernieren und jenen die das nicht tun zu finden.

Dazu wurde ein tröpfchenbasiertes Mikrofluidsystem eingesetzt, wobei einzelne Zellen in Medium eingekapselt wurden, separiert durch Öl. Im Medium befand sich ein FRET Reporterpeptid dass die MMP Aktivität quantifizierte und Tröpfchen, die einen gewissen Fluoreszenzschwellwert überschritten hatten, wurden dielektrophoretisch sortiert. Die Zellen wurden aus positiver und negativer Population wiedergewonnen und könnten nun sequenziert werden. Zur Etablierung des Assays wurden die Zelllinien HeLa und HT-1080 verwendet, wobei letztere MMPs auf der Zelloberfläche exprimierte. Die Identifikation genetischer Unterschiede primärer Tumorzellen die diesen Phäntotyp verursachen könnte zu neuen Behandlungsstrategien führen.

Contents

Preface

Acknowledgments

I would like to thank my two supervisors at EMBL, Christoph Merten and Jan Korbel, for the opportunity of doing research in their groups, their ideas and support, as well the group members for introducing me to the techniques used in the respective labs and many helpful discussions. I would also like to thank my official supervisor from Graz University of Technology, Prof. Helmut Schwab, for allowing me to do my Master's thesis at EMBL, which was a great experience.

Abbreviations

- APMA - 4-amino-phenyl-mercuric acetate
- CTL - cytotoxic T lymphocyte
- DMEM - Dulbecco's Modified Minimal Essential Medium
- FACS - fluorescence activated cell sorting
- FADS - fluorescence activated droplet sorting
- FBS - fetal bovine serum (also: fetal calf serum, FCS)
- FCS - fetal calf serum (also: fetal bovine serum, FBS)
- Glc - Glucose
- MMPs - matrix metalloproteinases
- NK cell - natural killer cell
- PBS - phosphate buffered saline
- PDMS - polydimethyl siloxane
- PEG - polyethylene glycol
- PET - polyethylene

- PFO - perfluoro octanol
- PFPE-PEG - polyfluoro-polyether polyethylene glycol
- PMT - photo multiplier tube
- PTFE - polytetrafluoroethylene
- RFU - relative fluorescence unit
- RPMI - Roswell Park Memorial Institute medium
- TGF - transforming growth factor

Part I

Introduction

1 Tumour biology

Cancer is a heterogeneous disease, given rise by the malignant transformation of cells that in turn gain the ability to proliferate to a point that is detrimental to the organism they reside in. The disease has claimed many lives, in wealthy countries second only to cardiovascular diseases. Most patients with cancer die not because of the primary tumour, but the dissemination of individual tumour cells that colonise distant sites to form metastases. For a malignant cell to be able to detach from a tumour and to subsequently found metastases in foreign tissues, it needs to attain certain properties [1]. A schema of the progression from a neoplasia to invasive disease and metastasis is shown in figure 4.

The cells comprising a tumour are heterogeneous. This means that many different cell types make up the tumour tissue, yet only a part of those actually are cancer cells (cf. figure 1). These not only have a different phenotype, but also differences in their genome due to the cancer cells acquiring evolutionary favourable traits during malignant transformation. Consequently, cancer cells do not act on their own but require a complex interplay with the surrounding tissue to provide them with nutrients, growth factors, and other chemical compounds. The population of cancer cells within a tumour is now thought of being maintained by a subpopulation of cancer stem cells [2].

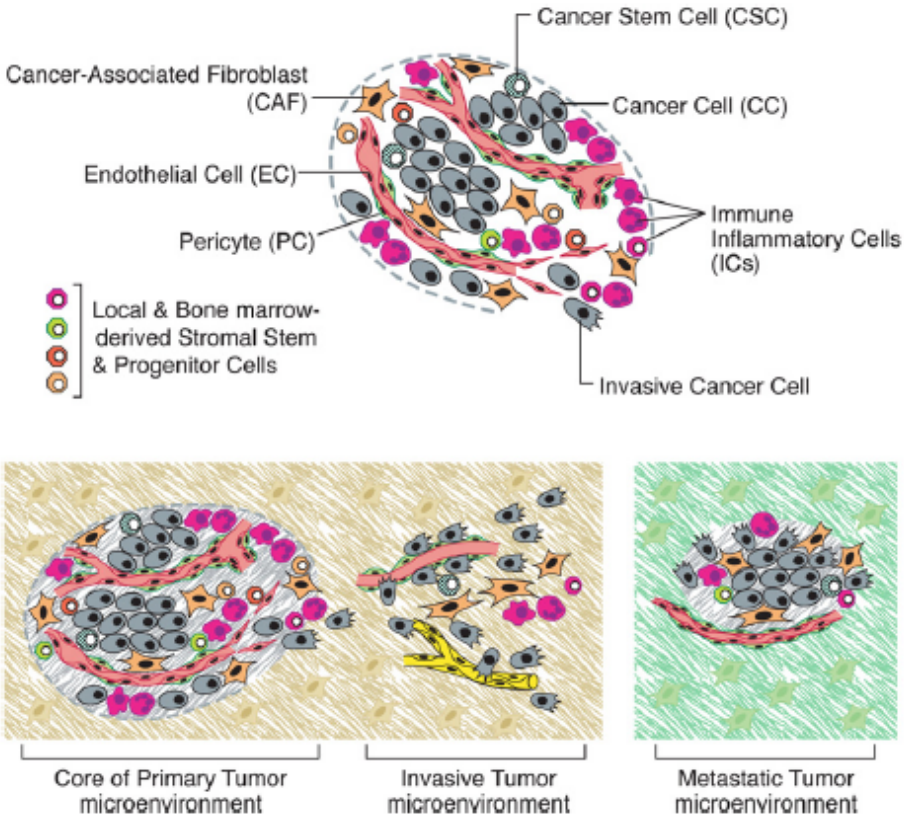

Figure 1: Illustration of the tumour microenvironment in primary neoplasia, invasive tumours, and colonisation at the metastatic site. The tumour does not consist of only cancer cells but a variety of different cell types, most of which are not cancerous themselves but promote cancer progression by reciprocal signalling with the cancer cells [1].

1.1 Characteristics of malignant transformation

In one of the classic publications in tumour biology, Hanahan & Weinberg proposed certain "hallmark" capabilities in year 2000 [3] that cells need to evolve in order for them to become cancerous. With new evidence mounting in the last decade, they reiterated their analysis in 2011, which is once again a comprehensive study of available literature knowledge on tumour development [1]. An overview over these hallmarks as well as approaches to treat them individually is shown in figure 2. Details are summarised below.

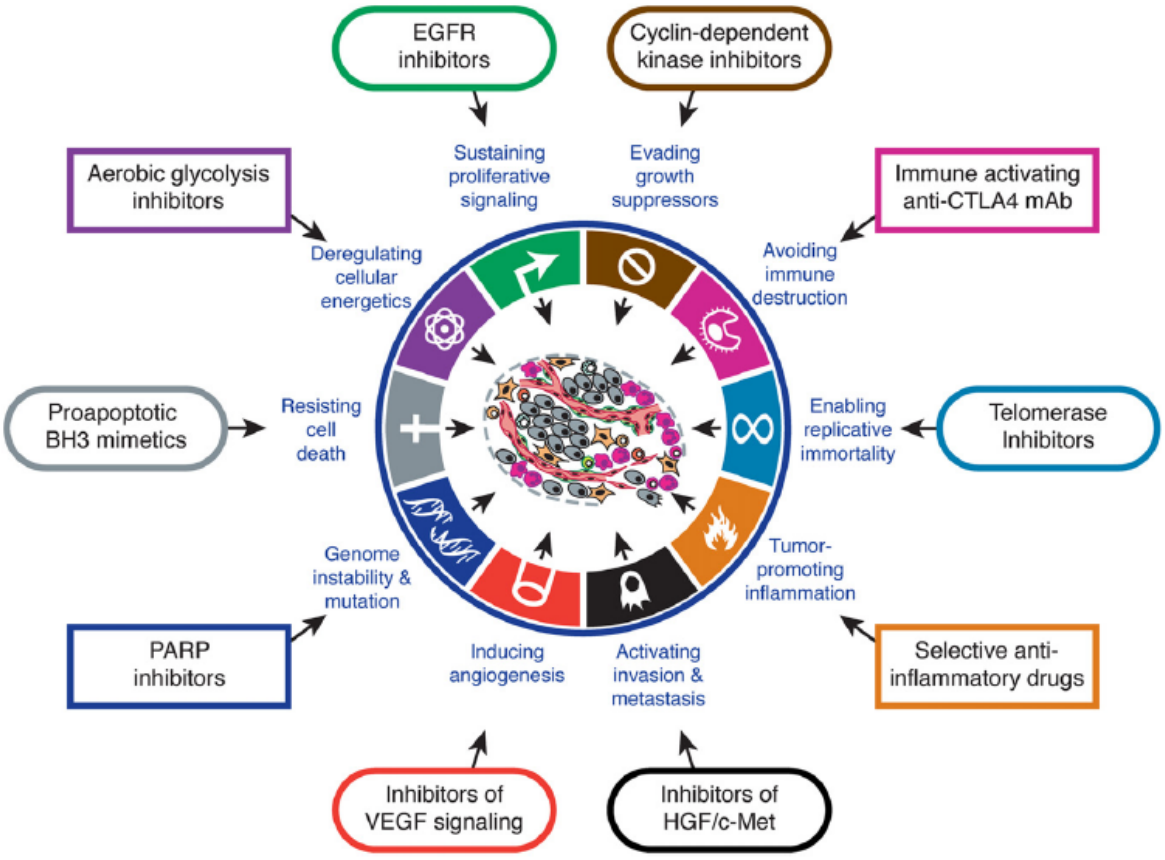

Figure 2: The hallmarks and enabling characteristics of cancer development and treatment approaches [1]

1.1.1 Sustaining proliferative signalling

Autonomous cell growth is the defining feature of all neoplastic cells, both benign and malignant. Unlike normal cells that tightly control cell cycle regulation, they often do not require mitogenic growth signals to enter an active state of proliferation. Those signals are transduced into a cell by a variety of transmembrane receptors, typically with an intracellular tyrosine kinase domain. Cancer cells have multiple possibilities to acquire proliferative signalling [1]. One possibility is for them to become more sensitive to the growth signals that are already present, *e.g.* by overexpressing the corresponding receptors. Another possibility is that the cells acquire the ability to produce growth factors themselves and in turn become entirely self-sufficient [4, 5]. Finally, cells can also

stimulate their neighbours to produce increased amounts of growth-promoting signals that support them in their proliferation [6, 7].

1.1.2 Evading growth suppressors

In addition of cancer cells to proactively being able to sustain their proliferative state, they also need to be able to evade signals that normally mediate cell cycle arrest. One example of such a checkpoint being derailed is the loss of contact inhibition, which causes normal cells to stop dividing when their density reaches a threshold [1]. The genes and proteins that are responsible for cell cycle arrest are generally known as tumour suppressors, the two most well-known are p53 and pRB. The RB protein is a general gatekeeper that integrates a multitude of signals to decide whether to proceed with or halt the cell cycle [8, 9]. Complementary, p53 is a stress and abnormality sensor that can halt the progression of the cell cycle until these conditions are normalised. If they can not be, the protein is able to trigger apoptosis. Both of these proteins, however, are not acting on their own but are a part of a larger regulatory circuit with some degree of redundancy [1].

1.1.3 Resisting cell death

Induced cell death is controlled by a counterbalance of pro- and antiapoptotic members of the Bcl-2 family. The archetype including its closest relatives (Bcl-xL, Bcl-w, Mcl-1, A1) are inhibitors of apoptosis, whereas two proteins of the same family (Bax and Bak) mediate the opposite effect [10]. Tumour cells have evolved a variety of strategies for evading the induction of apoptosis. For example, the loss of p53 is a common trait that eliminates a critical DNA damage sensor [11, 12]. Others include increasing the expression of antiapoptotic regulators or survival signals, or downregulating their

proapoptotic counterparts [1].

1.1.4 Enabling replicative immortality

Primary cells that are propagated in culture usually show a senescent phenotype after repeated cycles of cell division, where they are still viable but their further proliferation is blocked. Some cells in a population manage to circumvent this barrier, but the great majority then fall victim to a phase called *crisis* and die. On rare occasions, a small number of cells escape both barriers and exhibit unlimited proliferative potential. In this process called *immortalisation*, cells have found a way to maintain telomere lengths whose shortening has been implicated in the induction of senescence and crisis [13].

However, there are other signalling pathways that have been implicated in the same process and telomerase activity might have other unrelated proliferative effects as well [14].

1.1.5 Inducing angiogenesis

Like normal tissues, tumours require a constant supply of nutrients and oxygen as well as purging of waste products for them in order to survive and proliferate. Therefore, the tumour cells induce neoplastic generation of vasculature, in a process termed *angiogenesis,* to an extend that is far beyond that of physiological tissue [15]. The primary factor responsible for this process the the vascular endothelial growth factor (VEGF) that can be upregulated by both hypoxia and oncogenic signalling [16]. Another strategy is to free VEGF ligands that are sequestered in the extracellular matrix by matrix-degrading proteases (*e.g.* MMP-9) either directly or by inducing its expression in neighbouring cells [17].

1.1.6 Activating invasion and metastasis

Tissue invasion and metastasis is broadly regulated by the transition of cellular phenotypes from, epithelial to a mesenchymal. This process has been termed *epithelial-mesenchymal transition* (EMT) and is central to tumour progression [18, 19, 20]. One of the best characterised markers is the loss of the cell-cell adhesion molecule E-cadherin by cancer cells [21, 22], which is supplemented by the upregulation of the migratory phenotype N-cadherin [22]. A set of transcription factors is responsible for EMT process (Snail, Slug, Twist, and Zeb1/2), some of which have been found to elicit metastasis when ectopically expressed in cancer cells [23, 24].

Recently, it has been suggested that cell dissemination might be an earlier event and cancer progression that occurs before the cells have acquired their full metastatic potential, lead to by the discovery of circulating tumour cells in localised disease [25].

1.1.7 Emerging characteristics: deregulation of cellular energetics and avoiding immune destruction

While the properties described in section 1.1.1 to 1.1.6 have been known and investigated for a long time [3], two more emerging properties have been observed in cancer pathogenesis: the deregulation of cellular energetics towards a more glycolysis-centric metabolism thereby further promoting tumour growth and cell proliferation [26], and evading immune destruction by mechanisms that are still largely unknown although they have been suggested to include positive selection of weakly immunogenic tumour cells [1] or inactivating cytotoxic T lymphocyte (CTL) and natural killer (NK) cell function by secreting *e.g.* TGF-beta [27, 28] and other immunosuppressants [29, 30].

1.2 The role of Matrix Metalloproteinases

The family of matrix metalloproteinases (MMPs) consists of over 20 related enzymes that degrade a variety of extracellular matrix components. They all share highly conserved domains including an N-terminal activation domain and a catalytic zinc binding domain with three histidines as coordinating residues. In its inactive form, the cysteine of the activation domain coordinates the zinc atom as well and thereby inhibits function, explaining why activation of the enzyme requires proteolytic cleavage of this residue. The type of proteins also has a signal sequence that targets them for secretion or insertion into the plasma membrane [31].

MMPs have been shown to not only act in the process of tissue degradation, but also mediate cellular communication between the tumour cells and their microenvironment. A variety of cell types have been shown to produce MMPs in a physiological context, among which are cells of the immune system (Neutrophils, Macrophages, Lymphocytes, Dendritic cells, and Mast Cells), but also structural cells (Fibroblasts, Endothelial Cells) and non-terminally differentiated progenitor cells [17]. Categorised into different subtypes, the role of MMPs is diverse: they initiate proteolytic cascades, affect growth signals, regulate apoptosis, remodel the vasculature, induce function in immune- and adipoetic cells, and actively participate in tissue degradation [1, 2, 17].

Three MMPs have been shown to be able to cleave interstitial collagens (MMP-1, MMP-8, and MMP-13), and two (MMP-2 and MMP-9) are capable of degrading the basement membrane type IV collagen, albeit they exhibit more activity towards gelatins. The latter two MMPs are also responsible for cleaving fibronectin, laminin, and elastin. Two further MMPs (MMP-3 and MMP-10) have been shown to degrade proteoglycan components of the extracellular matrix (ECM) [31].

1.3 Prostate cancer as a model system

1.3.1 Prostate biology

The prostate is a secretory organ, which means that it consists of a stromal and a luminal compartment. Cells in the stroma exhibit a mesenchymal phenotype, while the ones in the luminal compartment are of epithelial origin. Androgen-receptor (AR) dependent signalling has an important role in cell differentiation and secretion of PSA by luminal cells. Cells of the epithelium include basal cells, luminal cells, and neuroendocrine cells. The cells of the stroma, as well as luminal cells and their intermediate precursors are AR-positive, while basal cells are AR-negative. Multiple differentiation models have been proposed, with the basal cells either being progenitors of other cell types or each lineage having its distinct precursors. In general, basal cells express more markers of intermediary cells compared to luminal and neuroendocrine cells [32].

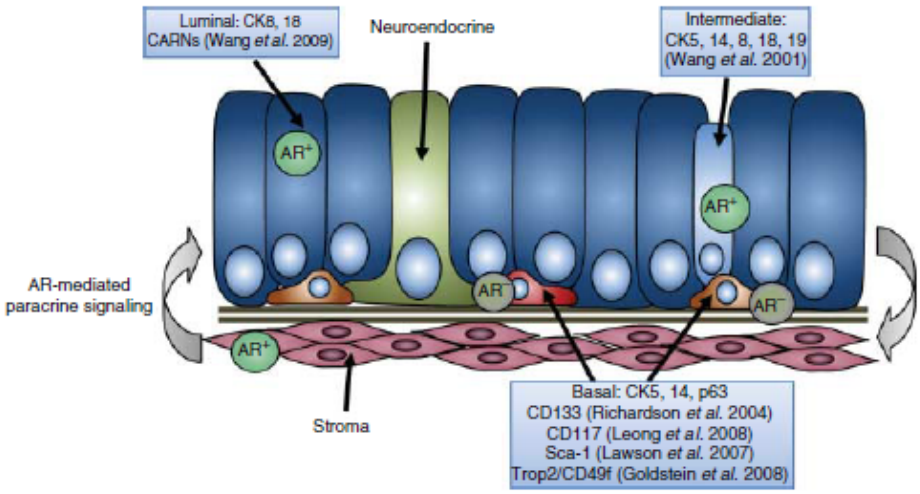

Figure 3: Illustration of different cell types in the prostate. It is composed of a stromal and an epithelial compartment that interact via AR-mediated paracrine signalling. The epithelium consists of basal, luminal, and neuroendocrine cells [32]. Cell surface markers [33, 34, 35, 36, 37, 38]

1.3.2 Disease progression and identification of prostate cancer cells

Most cancers of the prostate derive from the epithelium and are therefore carcinomas, as opposed to sarcomas that derive from the mesenchymal cells of the stroma. The former type accounts for over 80% of all prostate cancers [39], which is why the focus is on this type of cancer here.

In cancer development, normal epithelial cells start to proliferate and show the phenotype of a prostatic intraepithelial neoplasia that is spatially confined. These neoplasia can be benign and stay confined to their area or become malignant and invade the surrounding tissue, thereby becoming an adenocarcinoma. Diagnosis usually occurs when adenocarcinoma have already invaded surrounding tissue. Treatment includes surgical removal of the tumour and androgen deprivation therapy, which inhibits prostate cell proliferation in general by block AR-dependent signalling. If the cancer progresses further, its cells become independent of androgen, exhibiting an "androgen independent" or "castration resistant" phenotype [39].

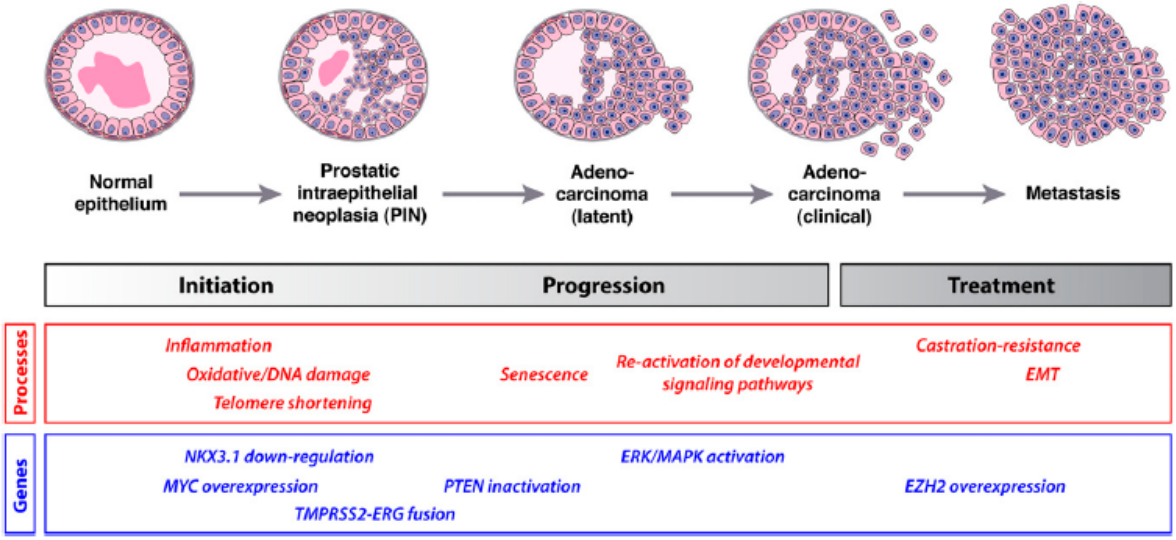

Figure 4: Disease progression with cellular processes and genetic markers indicated [39]

Because of the different cell types that could all be the origin of cancer, it is difficult

to determine the identity of prostate cancer cells by de-differentiation markers such as PSCA [40] or CD133 [35] because they are also expressed by basal cells and stem cells, respectively. It therefore seems best to use a panel of gene or expression markers (cf. figure 4) for identification.

2 Single cell screening

2.1 Reasons for investigating single cells

Cells present in a population have been observed to be phenotypically variable. This variability is mediated by a combination of intrinsic and extrinsic factors. One of these is of course the genetic differences present in a population, but cell signalling in a population context as well as general stochastic gene expression also play a role even when cells are genetically identical [41, 42, 43, 44]. In this case, their variability in gene expression and thus phenotype has been attributed to *extrinsic* and *intrinsic* noise [45].

The benefits and issues of single cell screening are particularly relevant when investigating a population of genetically distinct cell types, as is the case in the general study of heterogeneous populations of cells, *e.g.* the cells present in a tumour. One could for instance elucidate which genetic makeup is responsible for phenotypic traits when looking at the cells in isolation, thereby minimising cell-cell signalling, molecular crosstalk, and population context as cause of variability.

2.2 Challenges

High throughput biochemical or cellular assays have seen an evolution from 96 well plates to much higher densities and lower volumes [46]. For instance, Maffia *et al.* [47]

have carried out a luciferase reporter assays with T cells in 1536 well plates using just 3 uL of fluid volume. Oldenburg *et al.* [48] described a FRET-based cellular assay in 9600 well format using 0.2 uL volume for screening a drug compound library against matrix metalloproteinase (MMP) targets.

There are, however, technical hurdles when using robotic systems and micro- to picoliter well plates for those assays. One of them is the need to control capillary action [49] and sample evaporation [46] in systems that have a high surface-to-volume ratio. Another issue is reaching the accuracy limit for today's low volume liquid dispensing machines [46].

Recent developments in microfabrication of channel-like structures in which those assays could be performed might trigger a paradigm shift in high throughput technology. The establishment and application of this technology is currently pursued in both academia and industry [46] and has yielded numerous publications to date, some of which are listed in section 3.1.

3 Microfluidics

Microfluidics is a laboratory technique that allows for working with and manipulating low volumes of fluids in microchannels with dimensions of tens to hundreds of micrometers. Today, they are mostly manufactured as a negative print of polydimethylsiloxane (PDMS) on a structured surface. These devices have the potential to decrease manual labour as well as cost for the ingredients needed in biochemical assays, as it operates on very small volumes comprising nano-, pico-, or even femtoliters due to which they enable single cell assays. There are two main approaches taken with these devices, continuous flow and two-phase (using droplets generated in an water-in-oil emulsion) assays [46, 50].

While miniaturisation can expand the capability of existing chemical or biological assays, it does not change the nature or mechanism by which they occur. However, parameters like molecular diffusion or mass transport are affected by the assay scale, and those are the parameters that enable drastic increases in throughput. Microfluidics is one field of science which utilises the increased importance of those processes on smaller scale and it is set out to outperform currently used robotic fluid handling [51].

Besides increased reaction speed because of better diffusion efficiency, one of the most striking differences between macro- and microscale fluid systems is that the flow is governed by pressure gradients, viscous forces and low inertia, resulting in a turbulence-free laminar flow with low Reynolds number [52]. This has the effect that, for instance, two streams can flow adjacent to each other while mass transport between them is only influenced by diffusion, not mixing of the streams.

3.1 Techniques

3.1.1 Continuous flow microfluidics

Continuous flow microfluidic systems have been used for many applications. These include on-chip PCR [53] and electrophoresis [54], and investigating the effects of spatio-temporal perturbations on single cells [55, 56] or tissues. An example of the latter is the investigation of patterning in drosophila embryos [57]. Bacterial, yeast [58, 59], and mammalian [60] cells have been cultured on these devices, but also whole organisms of *e.g. Caenorhabditis elegans* [61]. Applications have been scaled up to investigate the effect of chemical or protein pulses or gradients on populations and sub-populations of cells using fluorescence microscopy [62, 63] and scaled down to probe the interaction between single molecules of DNA and their binding proteins [64].

Recently, the technology was used for single cell haplotyping [65], mapping recombin-

ation events in single human sperm cells using low-coverage whole genome sequencing [66], and even quantifying the proteome and transcriptome of individual *Escherichia coli* cells with single-molecule sensitivity [59].

3.1.2 Droplet-based microfluidics

The general idea of droplet-based microfluidics is to create an emulsion of aqueous droplets in oil that can act as inert microcompartments in which chemical or biological assays can be run [50]. The low volume of droplets combined with the speed at which they can be generated is unrivalled from robotic technologies.

While microfluidics using droplets is less established than continuous flow systems, it has already produced a number of success stories. After the first time it was shown that mammalian suspension- as well as adherent cells could be encapsulated in droplets and cultured for a couple of days [49], it became possible to quantify the activity of proteins secreted by those cells, as well as the recovering the contents afterwards [67]. One of the most researched topics is antibody production and -screening from single cells using their encapsulation in droplets in either affinity-based or actual activity-based assays [67, 68, 69]. However, other types of experiments like directed evolution also have been shown to be compatible with droplet-based microfluidics [70, 71].

3.2 Chip fabrication and assembly

As shown in figure 5, the making of a chip starts with printing a designed network of channels on a photomask, where all translucent space will correspond to those later. The remaining surface is printed with a black colour that blocks UV light. A silicon wafer is prepared by pouring a viscous fluid, the photoresist, on it and spinning it at a speed that causes it to disperse uniformly at a desired height, discarding the rest. The

layer of photoresist is subsequently heated up and kept at high temperature for a while to make it solidify.

Afterwards, the photomask is put on top of the wafer with photoresist. The two layers are squeezed together and (1) UV light is shown upon it, hitting all the spaces where the photomask is translucent and making the photoresist solidify fully in these areas. The photomask is removed and the wafer put in a developing solution (2) where all the photoresist that was not exposed to UV light is washed away, leaving a wafer with the negative structures of the desired channel network [72].

To generate the actual chip, PDMS is mixed with its curing agent and (3) poured on top of the structures on the mold. Residual air bubbles in the polymer are removed by applying a vacuum and the mixture is heated up and incubated to polymerise and solidify. The resulting solid PDMS with the imprinted channel structures is then cut out and (4) peeled off. Biopsy punches are used to punch holes (5) where the tubing will later be connected, the surface is cleaned and plasma treated to generate free radicals thereon, and (6) subsequently bound to a glass slide yielding the assembled chip [72].

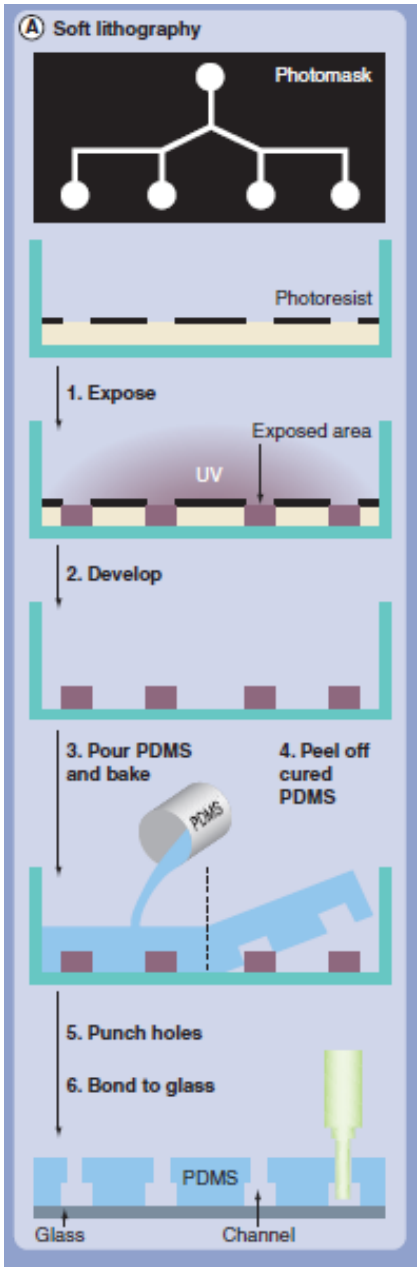

Figure 5: Overview over the chip generation process as described in section 4.3.1 to 4.4.2. A photoresist is solidified by shining UV light through a photomask, then PDMS is polymerised on the resulting structures, peeled off, and bound to a glass slide [72].

3.3 Basics of working with emulsions

3.3.1 Generating droplets, surface tension and surfactant

There are two approaches of droplet formation, either with a T-junction where water is injected into an oil stream, or by flow focussing, which is to have an aqueous stream being separated by splitting it with oil coming from either side. A schematic of the process is shown in figure 6. T-junctions appear to be simpler, and produce droplets that are a bit larger and touch the wall of the channel due to complete intermittance of the oil and the water phases. However, a drawback is that the droplet production rates can not keep up with those of flow-focussed systems. For flow-focussed droplets, there needs to be a constriction downstream of the point where the liquids meet in order to not have laminar flow of the two phases first that leads to uncontrolled polydispersed droplet formation later [50].

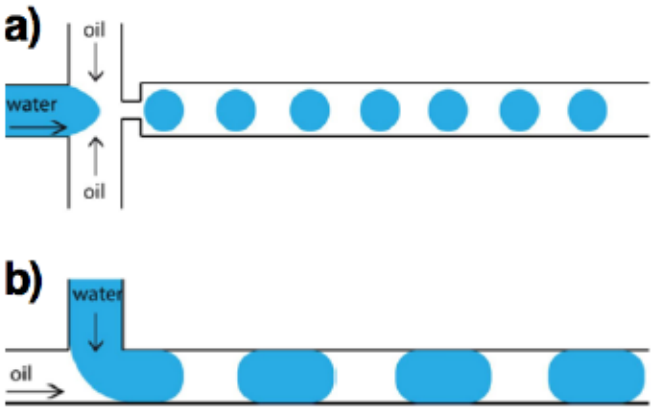

Figure 6: Techniques of droplet formation: (a) flow focussing and (b) T-junctions [73]

When two droplets of an oil-in-water emulsion come into contact, they instantly fuse because of the water's surface tension. In order to counteract this effect and to stabilise individual droplets as well as the emulsion as a whole, surfactant needs to be added to the oil before creating the emulsion. This surfactant needs to meet certain conditions

in order to be suitable for an experiment including living mammalian cells: it needs to stabilise the emulsion sufficiently while limiting micellular transport between droplets, and it needs to be compatible with living systems (*i.e.*, non-toxic at the concentrations used) [74]. One of the surfactants that has been previously shown to work well for cellular assays is PFPE-PEG [49].

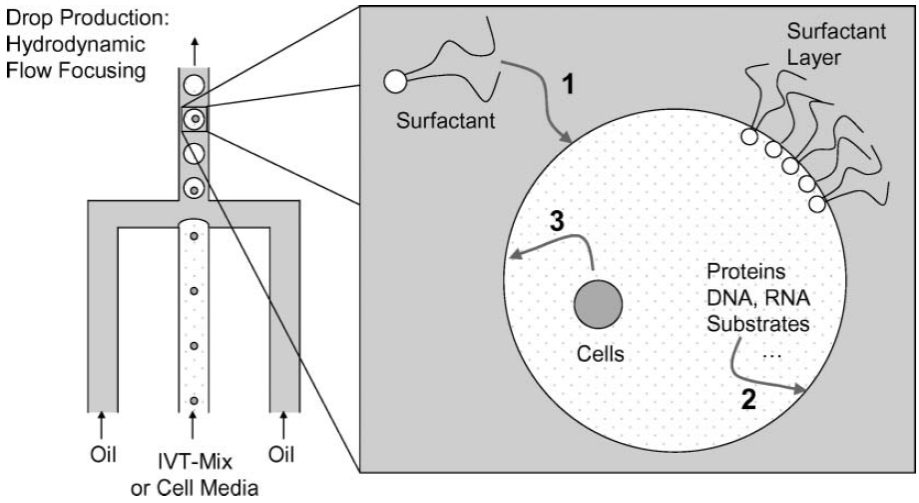

(a) Schema of cell encapsulation using flow focussing and the distribution of contents as well as surfactant within the droplet [74]

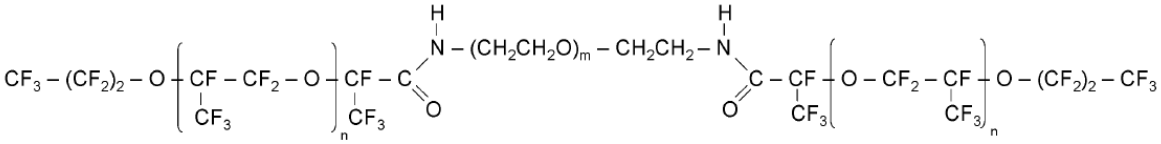

(b) Chemical structure of the PFPE-PEG surfactant [74]

Figure 7: Principles of cell encapsulation with droplets. (7a) Droplets of a water-in-oil emulsion used for the encapsulation of chemical or biological entities (proteins, DNA, cells, etc.). They are produced using flow focussing (left) and used to encapsulate cells, where a magnified view of the droplet (right) shows the distribution of molecules within. Surfactant molecules are enriched at the interphase between oil and water, while the droplet contents stay inside. (7b) PFPE-PEG consists of a long fluorocarbon tail (outer block) which mediates stabilisation in the oil phase and polyethylene glycol (centre) as the headgroup residing in the aqueous phase [74].

3.3.2 Fluorescence detection

Fluorescence markers in droplets need to meet certain requirements in order to be useful in this setting. For instance, they need to be excitable with the laser wavelengths used in the laboratory and their emission wavelengths have to pass the filters in front of the PMTs for a quantitative readout. Also, the fluorescent dye, or the product of an enzymatic cleavage should not be too hydrophobic in order to not leak into the oil or transfer between droplets (which has been shown to be the case with coumarin-based dyes, but not fluorescein-based ones [75]).

If the fluorescence is produced by an enzymatic cleavage of a substrate, this substrate should be stable without the presence of the enzyme and not be cleaved by unspecific activity of different enzymes.

Fluorescein The relatively small molecule used for initially setting up the system and that served as a proof-of-concept was fluorescein, which could be excited with the 488 nm laser and detected by the "green" PMT. It was encapsulated alongside medium or buffer to check if the design of the individual encapsulation and sorting chips generally worked, but could not monitor any kind of reaction taking place in the droplets.

FRET Fluorescence Resonance Energy Transfer has been know for a long time and follows a quite simple principle: a donor fluorophore, which is excited by light of a certain wavelength and emits photons at a lower frequency, and an acceptor fluorophore, which can be excited by the energy that the donor emits but that acts as a signal quencher that does not emit competing photons itself. As long as both fluorophores are in close physical proximity, light with the right excitation wavelength will not result in fluorescence. As soon as they are separated from each other, it fluorescence occurs.

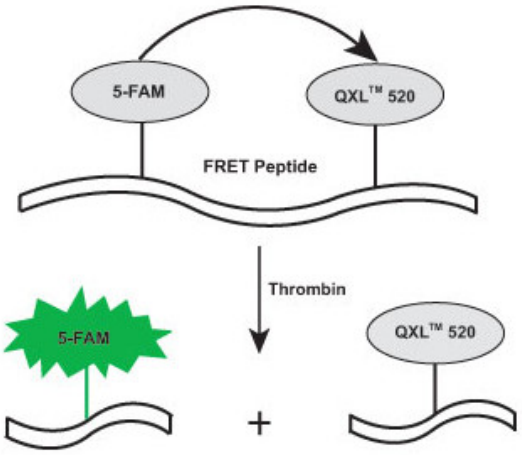

Figure 8: Operation mechanism of a FRET peptide. 5-FAM and QXL-520 were used in the experimental setup (AnaSpec)

The principle of the conducted screening for matrix metalloproteinases was to let them cleave a peptide with a fluorophore on one and a quencher on the other end. As long as the peptide remained intact, there was no fluorescence to be detected. Once cleavage occurred, fluorescence increases linearly with the amount of substrate cleaved.

3.3.3 On-chip and off-chip incubation of droplets

Droplets where all the reagents for an enzymatic reaction have been encapsulated need to be incubated for some time in order for this reaction to occur and sufficiently convert the fluorogenic substrate to a fluorescent product. If this happens in a matter of minutes, the droplets do not need to be taken off-chip but can be kept in large channels on the chip until the reaction is ready to be detected.

In most cases, however, the time that droplets can be kept on-chip is not long enough due to limited space on the device and increasing pressure when using a long delay line. This matters for instance when doing cell-based screenings, since the cells first need to express the enzymes that will later convert the substrate and is particularly relevant

if the enzymes are either secreted or surface-expressed and are degraded because of trypsinisation or tissue disaggregation. In this case, droplets need to be collected and incubated off-chip. Because they can not be screened in this state, they need to be reinjected into another chip afterwards.

One possible issue with prolonged incubation is that certain molecules, such as peptides or proteins, but also cells, have been shown to decrease the stability of an emulsion. This is why it is difficult to completely optimise the system without already encapsulating cells including the substrate peptide.

3.3.4 Principles of droplet sorting

After the reactions taking place inside each droplet of the emulsion had enough time to sufficiently complete, the fluorescent readout of each droplet can be detected using a laser/PMT setup (details cf. next section). In our case, as in the case with most cellular assays, droplets were collected and incubated, then reinjected. An example of how this looks like is shown in figure 9: the whole population is reinjected into an on-chip chamber where it is subsequently spaced out, detected, and sorted by dielectrophoresis [76].

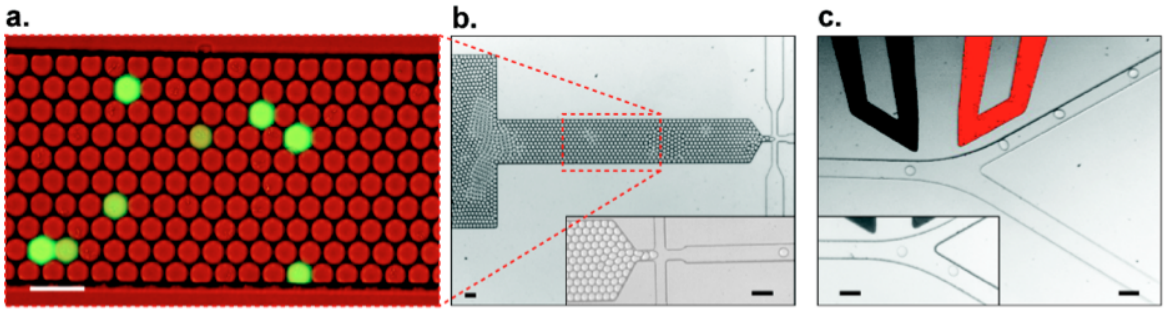

Figure 9: (a) The emulsion is reinjected into a chamber after incubation. The population of droplets contains a subset of fluorescence-positive ones, shown in green. (b) The reinjected droplets are subsequently spaced out by flow focussing of oil containing a low concentration of surfactant. (c) Spaced droplets default in the lower arm of the available channels at the junction, but can selectively be pulled in the upper one by applying an AC electric field. Scale bars 100 um [76].

Part II

Materials and Methods

4 Microfluidic device fabrication

4.1 Instruments and consumables

An overview of the workflow of creating microfluidic chips is shown in figure 5 and summarised in section 3.2. The instruments used were the following:

- Photomasks: Selba, Versoix, CH
- Spin coater: Laurell Technologies Corporation, PA, US
- Mask aligner: Reinraumtechnik Lanz, Konstanz, DE
- Diener Femto plasma oven: Diener Electronic, Ebhausen, DE
- SM818 UV oven: Blanko, DE
- PHD 2000 pumps: Harvard Apparatus, MA, US

- WPI pumps: Word Precision Instruments, FL, US

The workflow included the following consumables:

- Silicon wafers: Siltronix, Archamps, FR
- SU-8 photoresist" MicroChem Corporation, MA, US
- SU-8 developer: MicroChem Corporation, MA, US
- Sylgard 184 PDMS and curing agent: Dow Corning, Wiesbaden, DE
- Regular 3" x 5" glass slides: ThermoScientific, Roskilde, DK
- Harris UniCore biopsy punches (0.5 and 0.75 mm): Sigma-Aldrich, MO, US
- AccuSharp biopsy punches (1 and 3 mm): PSS, FL, US
- PTFE tubing TW24/HW30: Adtech, Stroud, UK
- PET tubing: : Adtech, Stroud, UK
- 1H, 1H, 2H, 2H Perfluorotrichlorosilane 97%, ABCR GmbH., Karlsruhe, DE
- Novec HFU7500 oil: 3m, MN, US
- Mineral oil: Sigma-Aldrich, MO, US
- PFPE-PEG surfactant: Sigma-Aldrich, MO, US
- Perfluorooctanol (PFO): ABCR, Karlsruhe, DE
- 1, 2, and 5 ml syringes: BD Plastipak, BD, Franklin Lakes, NJ, US
- Needles: BD Microlance, BD, Franklin Lakes, NJ, US

Software:

- AutoCAD: AutoDesk Inc., San Rafael, CA, US
- LinkCAD: Bay Technology, Burlington, IA, US

4.2 Chip design

The photomask later used for the lithography step was designed using AutoCAD 2010. With this programme, the outline of a 2D channel network was drawn and subsequently checked for connectivity with the LinkCAD software in order to ensure that there were no gaps in the outlines. Designs were sent for printing to the external company Selba. Finished photomasks had a resolution of about 5 um and were translucent in areas where channels were supposed to be created and black otherwise.

4.3 Mold fabrication

4.3.1 Photoresist

Silicon wafers were heated to 150°C for 10 minutes to allow for the evaporation of solvent residues and humidity. Photoresist and spin speed were chosen according to the desired channel height in the instruction manual. Photoresist was poured on the silicon wafer that was previously fixed on the spin coater, first for 10 s at 500 rpm to distribute the photoresist evenly and then at the correct speed for 40 s. The result of this process was a silicon wafer covered with a semi-defined height of photoresist on top of it. The wafer was subsequently heated to 65°C and 95°C ("soft bake") according to the height of the photoresist (cf. table 1) [72].

Table 1: Baking times of photoresist before exposure

Photoresist layer thickness [um]	Soft baking 65°C [min]	Soft baking 95°C [min]
25-40	0-3	5-6
45-80	0-3	6-9
85-110	5	10-20
115-150	5	20-30
160-225	7	30-45

4.3.2 UV exposure

Following the baking steps, the wafer was put in the mask aligner and the photomask put on it. The two layers were compressed and exposed to 350 W UV light for a defined time, where each second applied an energy amount of 10 mJ/cmš (cf. table 2 for the exact times). Where the UV light shined on translucent parts of the photomask, the photoresist solidified. After exposing, the wafer was again subjected to soft baking according to the time shown in table 3 [72].

Table 2: Exposure energy for given photoresist layer thickness. As the mask aligner's UV lamp has an energy of approximately 10 mJ/cmš/s, this value is divided by 10 to yield the exposure time in seconds.

Photoresist layer thickness [um]	Exposure energy [mJ/cmš]
25-40	150-160
45-80	160-215
85-110	215-240
115-150	240-260
160-225	260-350

Table 3: Baking times of photoresist after exposure

Photoresist layer thickness [um]	Soft baking $65°C$ [min]	Soft baking $95°C$ [min]
25-40	1	5-6
45-80	1-2	6-7
85-110	2-5	8-10
115-150	5	10-12
160-225	5	12-15

4.3.3 Structure development

The exposed wafer was then washed with SU-8 developer two times, where the developer was removed by spinning the wafer on the spin coater for one minute at 2500 rpm. The wafer was then soaked in developer again and put on a gel shaker for a couple of minutes, again depending on the channel height and type of photoresist. When the non-solidified

photoresist was washed away, it was washed with isopropanol. The structures created by the process were investigated under a stereomicroscope and further developed when necessary. In the end, the wafer was heated to $150°C$ and slowly cooled down in order to mend small cracks on the structure's surface [72].

The result of the mold generation process was a silicon wafer with solidified channel structures on top of it. The height of these structures was measured, as the height suggested by photoresist and spin speed were approximate and only more or less reflected the initially desired heights.

4.4 PDMS chip fabrication

The finished silicon wafer was put in a petri dish. PDMS was mixed 10:1 with its curing agent and poured on top of the wafer, until a height of approximately 4 mm was reached. The petri dishes were put on $65°C$ over night in order for the PDMS to polymerise. Subsequently, the part of the PDMS containing the structures was cut out with a scalpel and removed from the wafer, leaving the PDMS being imprinted with a negative image of the wafer's structures (cf. points 3 and 4 in figure 5). The wafer was cleaned with compressed air and could now be reused.

4.4.1 Hole punching

Biopsy punches were used to stamp holes in the PDMS where the tubings will be connected later. This was done starting from the side of the structures, in order to guarantee a precise positioning of the connectors. The PDMS was cleaned with compressed air and tape in order to remove small dust particles both from the surfaces and the newly punched holes (cf. point 5 in figure 5).

4.4.2 Plasma treatment

Both the structured PDMS and a glass slide were surface-activated using a plasma oven. Thereby, they were subjected to an oxygen-rich atmosphere for one minute where ozone was created that in turn created free radicals on the surface of both the PDMS and the glass slide. Following this process, the glass and PDMS could be bound molecularly by attaching them to each other (cf. point 6 in figure 5) and heating the resulting chip to $65°C$ for two minutes.

4.4.3 Silanisation

In the whole process of chip generation, a channel-like structure was created between the glass and the PDMS, with holes in the PDMS on defined inlets and outlets where tubing can be attached later. The channels were filled with a silanising agent and incubated for about five minutes in order to coat the hydrophilic PDMS structures with hydrocarbon groups using a 97% silane solution was diluted 1:100 in Novec oil and aspirated in a 1 ml syringe. A 0.22 um filter was used on the syringe to not let clumps of the silanising agent clog the channels. After this process, the chemical was flushed out with air.

4.5 Device and pump setup

Two different sizes of PTFE tubing were used, TW24 and HW30. TW24 had an inner diameter of 0.59 mm and a wall of 0.25 mm, yielding an outer diameter of 1.06 mm. HW30 had an inner diameter of 0.32 mm and a wall of 0.23 mm, yielding an outer diameter of 0.76 mm. The sizes of the tubings were corresponding to the holes punched with 1 mm and 0.75 mm biopsy punches, respectively.

In order to be able to infuse liquids into the microfluidic chip, this tubing was used in conjunction with plastic syringes on which hollow needles have been mounted. The needle size was chosen such that the system was properly sealed after inserting the needle into the tubing. Syringes were either filled before or after attaching the needle/tubing, depending on applying shear forces to the liquid was considered beneficial or harmful. The chip was connected when it was mounted onto the microscope. The tubing was flushed with liquid before connecting it to the chip to allow for easier insertion into the PDMS and to save time, as the pumps operated on a uL-mL/h scale. In case a pump was used in refill mode, *i.e.* to apply a negative pressure to the tubing, it was primed with Novec oil and used in infuse mode before in order to eliminate air bubbles in the system and allow for a more constant flow rate.

The flow rates of the pumps were chosen according to the current application and empirically optimised operating conditions and each of the syringes (cf. table 4) had a defined inner diameter that was entered on the pumps, with which they could calculate the plunger movement and per unit of time and push it correspondingly.

Table 4: Syringe selection guide. Using the diameter and the flow rate as inputs, the pumps calculated the speed by which they should move the plunger in a given amount of time.

BD Plastipak syringe	Inner diameter [mm]
1 ml	4.76
2 ml	8.66
3 ml	8.66
5 ml	12.06

4.6 Emulsion handling

4.6.1 Collection

As already mentioned in section 3.3.3, droplets under flow conditions can only be stored on-chip for a limited amount time and the amount of emulsion that fits on a chip is

limited as well. For these reasons, emulsions were collected in a 1 ml syringe where the plunger has been removed. To connect the syringe to the tubing, no needle was used because of the lower inner diameter resulting in higher flow speeds and thus droplet instability. Instead, a 3 mm PDMS piece with a 1 mm hole in the centre was punched and inserted in the front of the syringe. HW30 tubing was inserted into the PDMS using tweezers, until it fully penetrated the PDMS. This construct was silanised and left to dry over night. The syringe was fixed about 60 cm above the chip, already attached to a pump. Once the droplet formation on the encapsulation chip equilibrated, the collection syringe was connected to the emulsion outlet of the chip. In the syringe, a small fraction of aqueous phase (fused droplets) was found on top and the Novec oil on bottom (which has a density higher than water), with the emulsion gathering in between. When enough emulsion was collected, mineral oil was added on top to fill up the syringe completely. Afterwards, the pump was used to insert the plunger at a flow rate of 5000 uL/h beyond its critical insertion point. The syringe was then removed and put into an incubator for the cells to express their enzymes.

4.6.2 Reinjection

For reinjection, a flow rate of 1000 uL/h was used until the emulsion reached the chip again. As soon as droplets were visible in the chip channels, the flow rate was reduced to 15-30 uL/h, yielding 5-20 droplets per second with the droplet size and geometry used.

4.6.3 Breaking of emulsions and harvesting of droplet contents

On the outlet where the emulsion should be collected a short tubing with a length of about 10 cm was connected. On the other side, a hole was punched into the lid of an

Eppendorf tube filled with a small amount (approximately 100 uL) of aqueous phase and the tubing was inserted until it reached the bottom. The whole tube was put on ice while collecting the emulsion. After a while, it filled with oil on the bottom and emulsion on the interface between oil and aqueous phase. The emulsion was broken and its contents harvested by first removing the oil until 50 uL remained, adding 50 uL PFO and mixing the two phases by pipetting. PFO counteracted the effect of the PFPE-PEG surfactant and mediated droplet fusion with the aqueous phase. The sample was incubated on ice for about 15 minutes and shaken afterwards. 80% of the aqueous phase were taken out with a pipette and put into a well of a 96 well plate.

5 Mammalian Cell culture

5.1 Instruments and chemicals

Instruments and devices:

- 5810 R centrifuge: Eppendorf, Hamburg, DE
- HeraCell 240 Incubator: ThermoScientific, Roskilde, DK
- Neubauer Improved counting chamber: ThermoScientific, Roskilde, DK
- Isopropanol cell freezing container: Nalgene, Rochester, NY

The following media and consumables were used for cultivation of cell lines and tissue disaggregation:

- DMEM (Dulbecco's modified minimal essential medium) 4.5 g/L Glc: Gibco Life Technologies, Invitrogen, Carlsbad, CA, US
- RPMI 1640 (Roswell Park Memorial Institute medium): Gibco Life Technologies, Invitrogen, Carlsbad, CA, US

- Fetal Calf Serum (FCS): Gibco Life Technologies, Invitrogen, Carlsbad, CA, US
- FreeStyle Expression Medium: Gibco Life Technologies, Invitrogen, Carlsbad, CA, US
- T75 and T175 cell culture flasks: Nunc, ThermoScientific, Roskilde, DK
- 96 well plates: Nunc, ThermoScientific, Roskilde, DK
- Trypsin 0.05%/EDTA: Gibco Life Technologies, Invitrogen, Carlsbad, CA, US
- Accutase: Gibco Life Technologies, Invitrogen, Carlsbad, CA, US
- PBS (phosphate-buffered saline): prepared in-house
- PBS w/ 2 mM EDTA: prepared in-house
- Na-Pyruvate: Gibco Life Technologies, Invitrogen, Carlsbad, CA, US
- L-Glutamine: Sigma-Aldrich, MO, US
- DMSO (Dimethylsulfoxide): Sigma-Aldrich, MO, US
- Penicillin/Streptomycin: Gibco Life Technologies, Invitrogen, Carlsbad, CA, US
- Blasticidin: Invivogen, CA, US
- Hygromycin: Invitrogen, Carlsbad, CA, US
- Tetracyclin: Sigma-Aldrich, MO, US
- 15, 50 ml Falcon tubes: Falcon, BD, Franklin Lakes, NJ, US
- 1.5 ml freezing tubes: Nunc, ThermoScientific, Roskilde, DK
- T25, 75, 175 cell culture flasks: Nunc, ThermoScientific, Roskilde, DK
- 5, 10, 25 ml plastic pipettes with filter:
- 10, 20, 200, 1000 uL filter tips:
- Collagenase from *Clostridium histolyticum*: Sigma-Aldrich, MO, US
- Pronase from *Streptomyces griseus*: Roche Applied Science, Roche, Penzberg, Germany

5.2 Cell Lines

- HeLa T-REx: Invitrogen, Carlsbad, CA, US
- HT-1080: ATCC, Manassas, VN, US

5.2.1 HeLa T-REx

HeLa cells were isolated from the epithelial cells from the cervix of a 31 year-old adenocarcinoma patient in 1951. It is the oldest and most widely used cell line in culture. The special strain of HeLa T-REx cells used had a Flip-In T-REx system (Invitrogen) with a tetracycline-inducible promotor for GFP expression with Blasticidin and Hygromycin as antibiotic selection markers.

Blasticidin (200 mg/mL) and Hygromycin (2.5 mg/mL) solutions were aliquoted in their stock concentration, which corresponded to a 1000 and 500-fold compared to cell culture conditions (200 and 5 ug/mL, respectively). Tetracyclin was dissolved in 70% ethanol at a concentration of 5 mg/mL, which corresponded to a concentration of 5000-fold compared to cell culture conditions (1 ug/mL). Hygromycin and Tetracyclin were protected from light. For the first couple of passages, HeLa T-REx cells were cultivated with Hygromycin and Blasticidin in order for them not to lose their Flip-In GFP expression system.

5.2.2 HT-1080

HT-1080 cells were isolated in 1972 from connective tissue of a 35 year-old fibrosarcoma patient. Along with the MDA-MB-130, the HT-1080 is a standard cell line that is know to express extracellular matrix metalloproteinases (MMPs). It was used as a positive control for the bulk as well as on-chip assay for MMP activity. An initial

amount of cells was obtained from the German Cancer Research Centre (Deutsches Krebsforschungszentrum, DKFZ).

5.3 Cell culture techniques

5.3.1 Cultivation

As a cell culture medium, high-glucose DMEM supplemented with 10% FCS, 1% L-glutamine (if not already present in medium), and 1% sodium pyruvate to enhance attachment was used. 1% Penicillin/Streptomycin solution was added to avoid bacterial growth. The volume of medium used was dependent on the flask size, see table 5 for details. Medium was pre-heated to $37°C$ before use. Cells were seeded at an initial density of 1-4e5 and incubated at $37°C$ with 5% CO2 atmosphere saturated with water until they reached confluence. At any point, the medium was exchanged when the pH was decreasing too much because of cell metabolism (as indicated by phenole red turning yellow). This was necessary every 2-4 days, depending on the cell density already reached.

5.3.2 Splitting

At confluence levels, the cell lines were split at a subcultivation ratio of 1:4 to 1:10. Therefore, they were washed with PBS twice and detached with either EDTA, Trypsin/EDTA, or Accutase. In either case, medium was removed and the cells were washed with PBS before detachment. When using 2 mM EDTA, cells were incubated for 20 (in case of HT-1080) or 40 minutes (HeLa T-REx). For Trypsin or Accutase it was both 5 minutes, the former at $37°C$. The volumes added to a T75 flask were 10, 4, and 4 ml, respectively (see table 5 for a full list of volumes). Depending on the different

detachment methods, cells that were used for analyses either had their surface proteins partially removed (Trypsin), or most of them stayed intact (Accutase, EDTA). This is why the latter methods can be considered milder forms of detachment, while with the former, cells need more time to recover. Upon detachment with Trypsin, an equal volume medium was added before the centrifugation step that coated the protease's activity. Cells were centrifuged at 1000 rpm for 4 minutes. The supernatant was removed and they were resuspended in medium and seeded into new flasks according to their desired density.

Table 5: Cell culture volumes for different flask sizes, where the number following the T indicates the surface area. Medium: volume of medium used to culture cells, PBS: volume used to wash cells, Trypsin/Accutase/EDTA: volumes used for detachment.

Flask size [cm^2]	Medium [mL]	PBS [ml]	Trypsin or Accutase [mL]	EDTA [ml]
T25	5-6	5-6	1.5	5
T75	10-15	10-15	3	10
T175	25-30	25-30	5	20
96 well plate	0.1	0.05	-	-

5.3.3 Freezing

Freezing medium was prepared by adding 10% FCS (20% total) and 10% DMSO to already supplemented DMEM. It was aliquoted in 15 mL Falcon tubes, where the currently unused ones were stored at $-20°C$.

Upon first reception of the cell lines, they were expanded in two T175 culture flasks. When they reached confluence, they were trypsinised (cf. section 5.3.2) to yield a high total number of cells that were passaged for only a few times. 1 ml aliquots of about 1-2e6 cells/mL resuspended in $4°C$ pre-cooled freezing medium were transferred into 1.5 mL freezing vials. These were put in a cell freezing container filled with isopropanol and put in -80$°C$ over night, before storing them in the vapour phase of liquid nitrogen.

This ensured that they were cooled down at a rate of about $1°C$ per hour until they reached $-80°C$.

5.3.4 Thawing

When taking out freezing vials from storage in liquid nitrogen they were palm-warmed and put into a $37°C$ water bath as soon as possible to ensure quick thawing. They contents of one vial were transferred into a 15 mL Falcon tube filled with 10 mL medium. The cells were spinned down at standard centrifugation speeds and resuspended in 10 mL medium, which was transferred to a T75 flask for cultivation.

5.3.5 Tissue disaggregation

FreeStyle medium was prepared with 5 mg/mL Collagenase and 100 ug/mL Pronase, yielding the dissociation reagent. The medium was chosen because it was already available and does not contain FCS, which is known to block the activity of proteases.

Tissue samples were cut into pieces of about 3 mm in size using a sterile scalpel. These pieces were incubated in the dissociated reagent for two hours at $37°C$ in a gently shaking falcon tube. Depending on the progression of the digestion, up to an hour of incubation time was added.

Afterwards, the cells and remaining aggregates were centrifuged with 800 rpm for 5 minutes and washed in DMEM medium with 10% FCS for three times, discarding the supernatant. This ensured that all the enzymatic activity was gone and parts of broken cells were discarded. In order to discard cell aggregates and remaining undegraded tissue components as well, the suspension was filtered using a grid mesh with 22 um pore size.

6 Encapsulating cells in droplets

6.1 Instruments and consumables

Standard cell culture equipment (for details cf. section 5.1)

- PBS: prepared in-house
- Supplemented DMEM, RPMI medium or FreeStyle medium: Gibco Life Technologies, Invitrogen, Carlsbad, CA
- 5810 R centrifuge: Eppendorf, Hamburg, DE
- Neubauer Improved counting chamber: LaborOptik, Lancing, UK

Microfluidic equipment (for details cf. section 4.1)

- 1 or 5 mL syringe: BD Plastipak, BD, Franklin Lakes, NJ, US
- Hollow needle: BD Microlance, BD, Franklin Lakes, NJ, US
- TW24 tubing: Adtech, Stroud, UK

Additionally to this, a magnetic stir bar and stirrer were used:

- Magnetic stir bar and magnetic stirrer

6.2 Preparing the cell suspension

When the cells were used for either a bulk or a chip experiment, they were subjected to additional procedures after detachment and centrifugation (cf. section 5.3). They were resuspended in 10 mL of $4°C$ pre-cooled PBS and spinned down again with the same centrifugation speeds. This was repeated a second time to wash away any remaining small debris and secreted enzymes that may interfere with the assay afterwards. Before

the second centrifugation step, the number of cells was determined in a Neubauer counting chamber. After that, they were resuspended in a pre-cooled corresponding volume of either DMEM, RPMI, or FreeStyle medium to yield a final concentration of between 5e5 and 2e6 cells/mL. Resuspension medium was always filtered with a pore size of 0.22 um before using it.

In order not to let the cells settle down and clump together in the syringes, a magnetic stir bar was put into the syringe that was rotated by 250 rpm. The tubing between the stirred syringe and the chip was kept as short as possible, in most cases around 15 cm.

6.3 Chip design for encapsulation

6.3.1 Poisson encapsulation

Single cell encapsulation of human cell lines using flow focussing has been previously shown by using 660 pL drops and a channel geometry of 100 x 75 um. Starting from a suspension, the number of encapsulated cells has been shown to closely follow a Poisson distribution [49]. To maximise the number of droplets which contain a single cell, the authors have encapsulated dilutions of 6.25e5 to 5e6 cells/mL. A value between 1.25e6 has been shown to work best (62% empty droplets, 33% with single cells, and 5% with two or more cells) and corresponds to the maximum ratio of droplets with single cells but has a significantly lower abundance of double encapsulations compared to higher cell concentrations.

6.3.2 Deterministic encapsulation

More recently, there have been attempts to overcome statistical encapsulation by using microdroplets [77] or designs that make use of Dean forces in order to distribute the

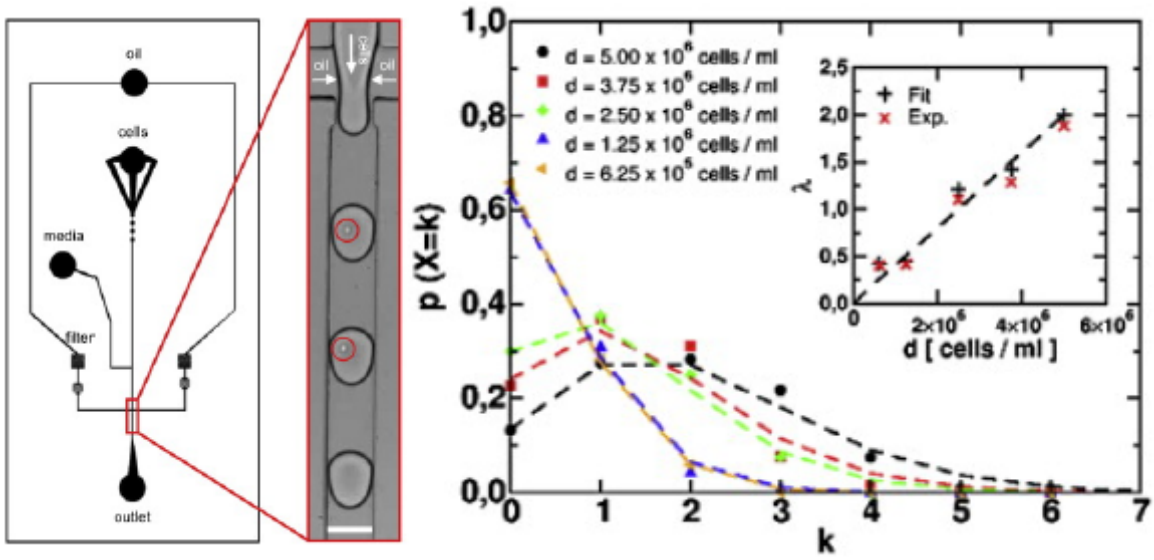

Figure 10: Design of a chip using flow focussing for cell encapsulation and the corresponding statistics of how many droplets are occupied with each number of cells [49].

cells evenly on curved channels [78]. While the former design required a high degree of sophistication, the latter only used spatial geometry to obtain this effect (albeit with a lower accuracy). With the curved channel device, the authors could show a ratio of 77% of droplets containing a single cell, 14% empty droplets and 9% with two or more cells. They mentioned, however, that this ratio dependent strongly on the exact concentration of the cell suspension as well as its homogeneity.

7 Fluorescence detection and sorting of droplets

7.1 Instruments and Consumables

Two workstations were equipped with the following instruments:

- Eclipse Ti microscope: Nikon, Tokyo, JP
- MotionBlitz EoSense Mini1 camera: Mikrotron, München, DE

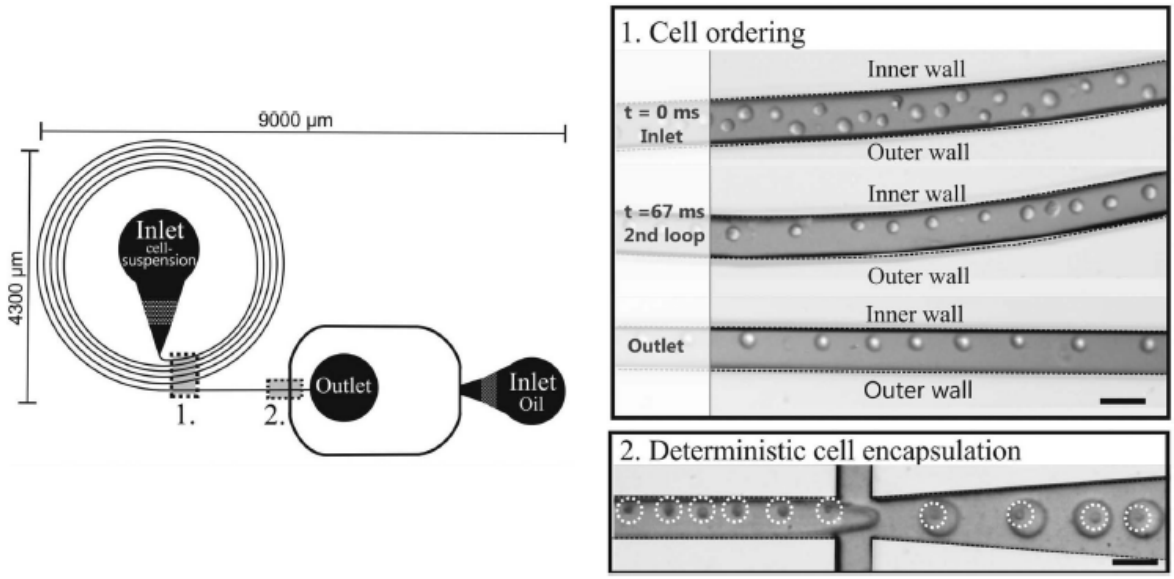

Figure 11: Dean-force based encapsulation on a curved microchannel [78]

- ORCA-05G fluorescence camera: Hamamatsu, Hamamatsu, JP
- TREK 623B High voltage amplifier: BFi OPTiLAS, Grobenzell, DE
- 488 nm laser: CVI Melles Griot, Albuquerque, NM, US
- HeraCell 240 Incubator: ThermoScientific, Roskilde, DK

The laser setup and the pulses of the high voltage amplifier were controlled using the following in-house LabView software:

- Laser control module (LabView, in-house)
- Analysis and Sorting module (LabView, in-house)

Chemicals that were used:

- Fluorescein: Sigma-Aldrich, MO, US
- 520 MMP FRET substrate XIV: AnaSpec, Eurogentec, Liège, BE

7.2 Workstation setup

7.2.1 Optics

Lasers were connected to the side of the microscope (for an overview of the whole workstation setup, see figure 12), enabling an excitation of fluorophores directly in the centre of the field of view. They were available with three different wavelengths on the workstations: 375, 488, and 506 nm. Those were controlled with a LabView module, written for particularly this purpose. An overview of the interface is shown in figure 13. Laser activation consisted of two steps, initialisation of the connection between the module and the laser itself and the individual on/off control.

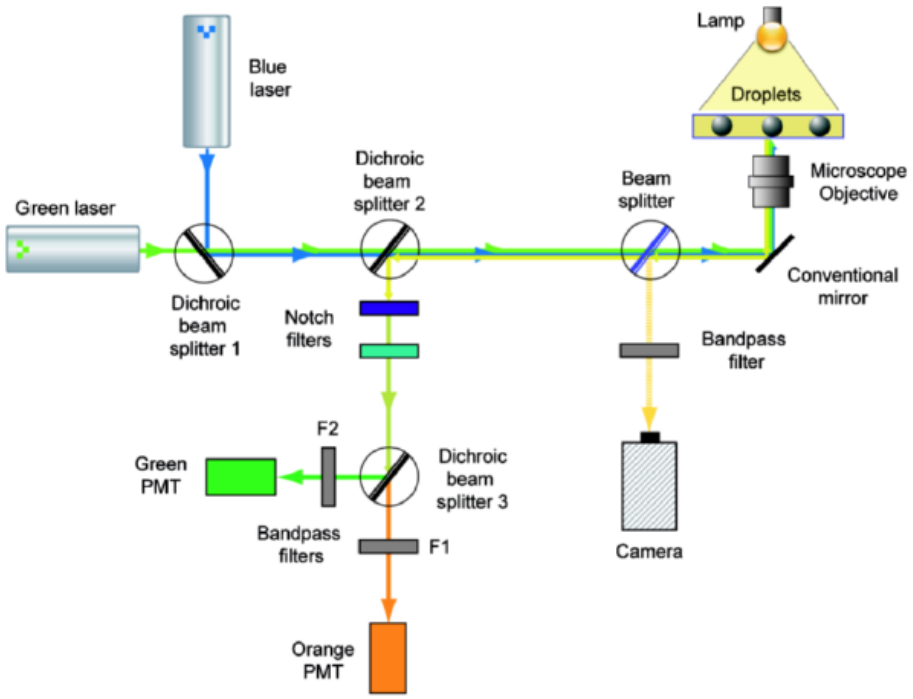

Figure 12: Schema of a microscope and laser setup of a microfluidic workstation [79]

When a fluorophore was excited with the laser, its fluorescence could be detected with photomultiplier tubes (PMTs), where the wavelength of interest could be constantly monitored. In the case with fluorescein being excited at 488 nm, it emitted green light,

i.e. the wavelength of about 520 nm. This is also the wavelength one of the PMTs was set up to detect. The LabView Analysis and Sorting module was used to determine the amount of photons from the PMT at a rate of 100 kHz. Once the signal exceeded a certain detection threshold, the amplitude of the signal (in millivolts PMT readout) and the time it stayed above this threshold ("width," in milliseconds) were measured and recorded.

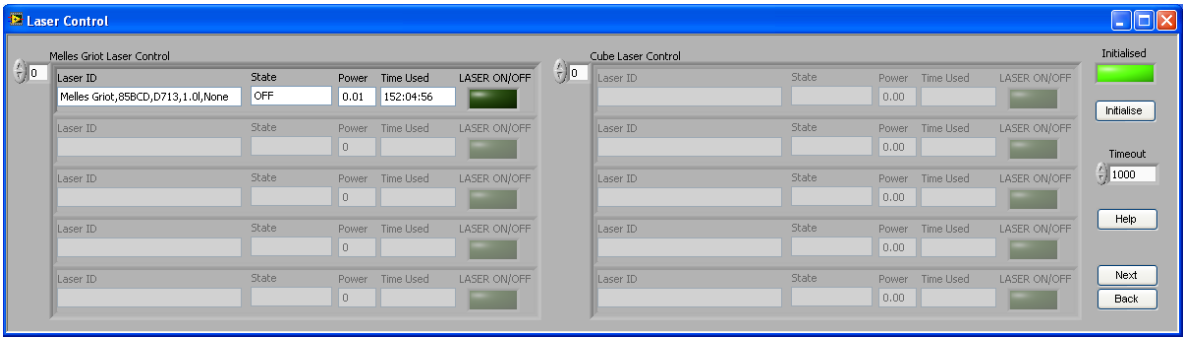

Figure 13: Laser control module

An overview of the "Live Read" tab in the Analysis and Sorting module can be seen in figure 14. The signals shown in this figure are placeholders for when the PMTs are turned on that also reflect the system being properly connected. PMTs for green, orange, and UV light are plotted in different colours and could be turned on or off individually in both linear scale and log-scale plots. Signal amplification could be achieved by setting an electrical gain in the system. The module reported the frequency by which the signal exceeded the before set threshold. Every pair of signal width and amplitude could be written to a file using the Record option.

Apart from the live read, the LabView module also showed a preview scatter plot (cf. figure 15) of width and fluorescence intensity, with a total count of detected droplets and those who were between gates the user could set. If a signal was within these gates, an electrical pulse that mediated the sorting mechanism could be applied.

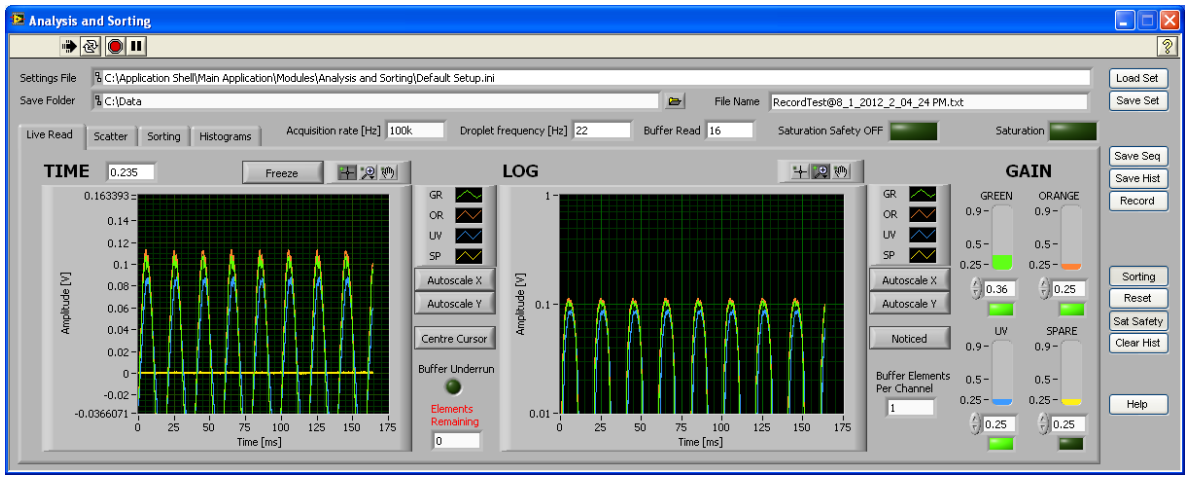

Figure 14: Signal detection in the Analysis and Sorting module

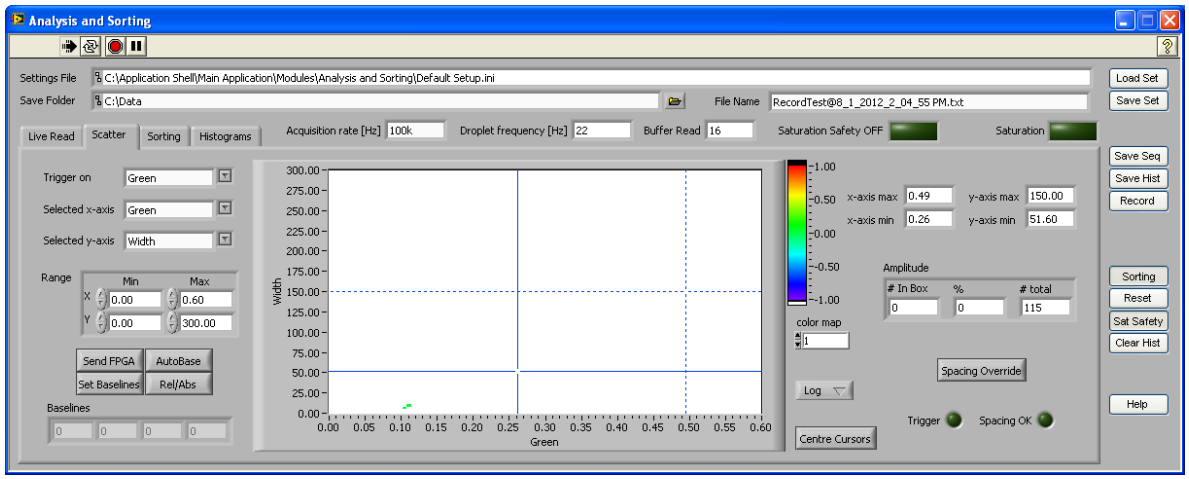

Figure 15: Histogram view in the Analysis and Sorting module

7.2.2 Dielectrophoretic sorting

According to the fluorescence amplitude and width, sorting gates could be set in which an electrical charge could be applied to the electrode that was soldered into separate electrode channels within the chip, next to a grounding electrode in an adjacent channel. When an electrical pulse was applied, the difference in conductivity between the oil and the aqueous phase lead to the formation of a dipole, which dragged the droplet closer to the electrodes.

With the sorting tab of the module (cf. figure 16), settings specific to the sorting procedure could be set. The pulse mode "triggered" thereby defined to only apply electrical pulses when desired, *i.e.* a fluorescent signal lay between the before specified sorting gates. The voltage specified was amplified by the high voltage amplifier by a factor of 1000. In this case, a voltage of 2.3 V results in a voltage of 2300 V being applied on-chip. Further options included:

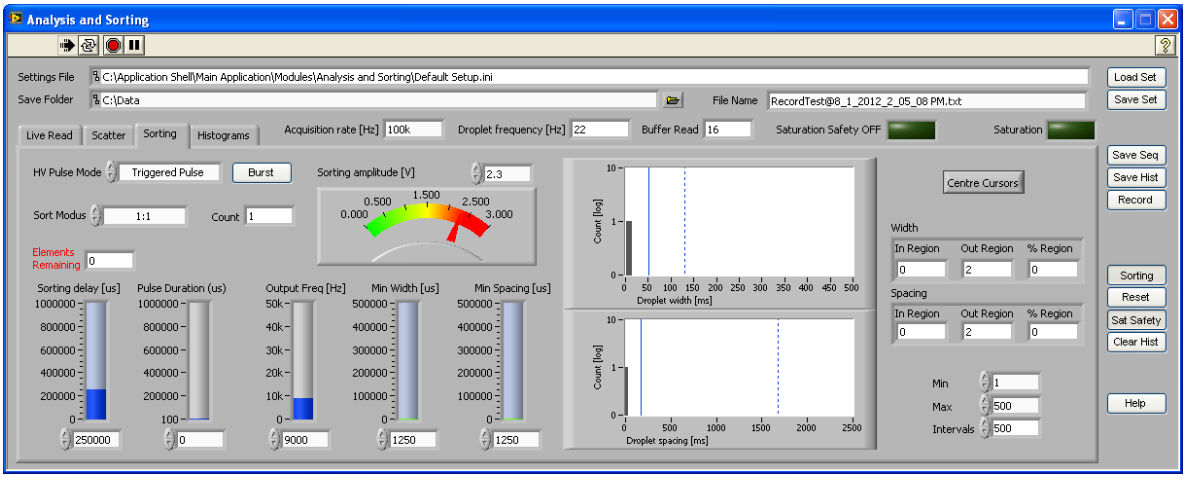

Figure 16: Sorting settings in the Analysis and Sorting module

- Sorting delay: the time delay between a signal being detected completely (*i.e.*, it fell below the detection threshold again afterwards) and the application of the electrical pulse
- Pulse duration: the duration for which a pulse should be applied; higher pulse durations hat a stronger pulling effect, but beared also the danger of pulling droplets preceding or following the current one as well as overheating of the electrode
- Output Frequency: the frequency in which the direction of the applied voltage changed per second
- Minimal Width: the minimal amount of time a signal needed to be above the detection threshold in order to be counted as a signal compared to background noise

- Minimal Spacing: the minimal time (distance) between the last signal and the current one for an AC pulse to be applied

Part III

Single cell screening for MMP activity

8 Rationale

In cancer, the physiological processes mediated by cells in a given tissue are derailed and at the initiation of this process MMPs play a crucial role. It is currently thought that the bulk of MMP production is realised by tumour-associated stromal cells, however, for cells in order to invade foreign tissues and metastasise they can no longer rely on their microenvironment. It is thus our working hypothesis that tumour cells need to produce and secrete MMPs themselves to (a) control the microenvironment in which they reside in and (b) be able to degrade tissue at the invasion site.

Cell lines derived from tumours predominantly do not secrete MMPs, but some do. With this information, one can conclude that either in a special subtype of tumours the cancer cells secrete MMPs, or that in most tumours some cancer cells do. In reality, the effect seen is likely a mixture of both. However, the latter is more realistic in a sense that cancer cells need to maintain their microenvironment and invade tissue in order to metastasise. It can further be argued that cells expressing MMPs contribute considerably to the establishment and maintenance of this microenvironment and MMP secretion by cancer cells is a marker of tissue invasion.

Treatments that target and thereby inhibit MMP function have been suggested, some of which have made it into clinical trials. However, because of the important physiological role of the same enzymes, drug development for MMP inhibitors is a difficult task [31]. Knowing how much the actual cancer cells, as opposed to their microenviron-

ment, contribute in the cellular crosstalk that is a network of, among others, MMP signalling might provide novel insight in the regulation of the microenvironment and tissue invasion by cancer cells.

9 Objective

Being able to expose genomic determinants that cancer cells evolved in order to actively take part in this crosstalk compared to those which do not might yield novel approaches for disrupting the cycle of cell growth, inflammation, tissue degradation, and freeing of additional nutrients and growth factors that ultimately result in tumour progression.

We therefore propose to develop a screening platform using microfluidics technology for single cell analysis of cell culture as well as primary cells that will reliably test and sort a small fraction in a large population of cancer- and microenvironmental cells. The model system of choice will be cell lines that do or do not secrete MMPs, as well as primary prostate cancer samples. For the latter, we will use previously known determinants of cancer cells to identify them in both the MMP- positive as well as MMP-negative population. We would ultimately like to be able to analyse the genomes of both variants to discover evolutionary principles in which they develop as well as provide potential targets for drug design, but that may have to be left to a follow-up project due to time constraints.

10 Experimental Setup

While the general materials and methods used to obtain the results listed later are already described in the corresponding section (part II), this section describes the exact experimental setup and measurement parameters that were used to obtain these results.

Enzymatic assays were carried out using recombinant human MMP-1 and all used a fluorogenic broad-range substrate (cf. section 7.1).

10.1 In-bulk assays

As testing and optimisation of assays carried out on microfluidic devices is time consuming and error-prone, the general approach taken was to first make sure observe the desired effects with bulk assays on a population level, using mostly 96 well plates. As soon as everything was shown to work in bulk, the more complex task of optimising the system for the microfluidic platform was performed.

10.1.1 Enzymatic assays

As the recommended wavelengths for excitation and detection of a cleaved MMP substrate were 490 ± 20 and 520 ± 20 respectively, an emission scan was conducted in order to confirm the substrate working with a slightly different and less broad wavelengths that resembled the laser and PMT setup more closely, *i.e.* 488 ± 5 and 520 ± 5 nm.

For the enzymatic assay, recombinant human MMP-1 was activated by incubating 20 uL of 50 ug/mL MMP-1 and 1 mM APMA at $37°C$ for two hours. 120 uL aliquots of PBS and DMEM 4.5 g/L Glc with 10% FCS were added to eight wells each in a 96-well plate. Half of either also contained 25 ng/mL activated MMP-1, making a total of 4 replicates in each condition. Reactions were started by adding 30 uL of 20 uM broad spectrum MMP substrate to the reactions, yielding a final assay concentration of 5 uM substrate and 20 ng/mL enzyme. In order to start the reactions at the same time, multi-channel dispenser pipettes were used.

Fluorescence measurements were taken at an excitation wavelength of 488 ± 5 nm and detected at an emission wavelength of 520 ± 5 nm. The signal was integrated

over 40 us with a gain manually set at 55 (45 after one hour) for three times and averaged. Measurements were taken every 5 minutes for a total of 2.5 hours. Incubation temperature was $25°C$.

10.1.2 Cellular assays

Aliquots of 800 uL of the following buffers or media were prepared:

- PBS
- PBS with 5% FCS
- DMEM 4.5 g/L Glc
- DMEM 4.5 g/L Glc with 10% FCS
- RPMI 1640 with 10% FCS
- FreeStyle medium

To each of the media listed, 2 uL of broad spectrum MMP substrate with a concentration of 1 mM in DMSO were added and the solution was mixed. Aliquots of 90 uL each were distributed in eight wells of a 96-well plate, yielding a total of 48 wells filled with 6 different media or buffers. A blank using PBS (two replicates), as well as suspensions of HeLa T-REx and HT-1080 cell lines (three replicates each) with a concentration of 7.5e5/mL were prepared and added into the adjacent wells of the 96-well plate to be able to start the reactions later with minimal time delay by using multichannel dispenser pipettes using a volume of 30 uL, yielding either none (blank) or 22500 cells per well. The final assay concentration of the substrate was 1.875 uM. Cell lines were trypsinised from their culture flasks (details cf. section 5.3.2), counted for an approximate dilution, washed two times with PBS, and counted again to prepare an accurate dilution. Before transferring the cells into the wells or between the wells, they were mixed by pipetting at least three times in order to ensure a homogeneous suspension.

Fluorescence measurements were taken at an excitation wavelength of 488 ± 5 nm and detected at an emission wavelength of 520 ± 5 nm. The signal was integrated over 40 us with a gain manually set at 55 for three times and averaged. Measurements were taken every 10 minutes for a total of 5 hours. Incubation temperature was $37°C$.

10.2 Cell encapsulation

One of the crucial points to consider if one wants to run cellular screens in droplets is to actually be able to encapsulate roughly one cell in each droplet, without them clumping together or dying because of mechanical or chemical stress. The stochastic nature of standard cell encapsulation has been discussed in section 6.3.1, and it was previously shown that a ratio of about 2/3 empty droplets and 1/3 single cell containing droplets could be achieved with a low (approx. 5%) amount of droplets containing two or more cells [49].

Droplet size and concentration of the cell suspension could be varied, but the always had to be matched to each other. Smaller droplets are more stable, but require higher cell concentrations to conduct a screening that has a sufficient number of droplets containing cells, which may not always be available. Also, cells only have a limited supply of nutrients inside each droplet, thus imposing a minimum droplet size depending on how long they should be kept inside. More aggressive disaggregation procedures and stirring has considerable impact on the occurrence of cell clusters, but also on cell viability. The substrate concentration inside the droplets needs to be high enough to yield a detectable signal, but also destabilises droplets.

10.2.1 Disaggregation procedure

The three methods for cell detachment, as well as one additional method for tissue disaggregation were previously described. Detachment with EDTA was most gentle, followed by Accutase treatment and then Trypsin.

Encapsulations were tried with all three methods of detaching the cells from the culture flasks. EDTA was found to take a long time (20 to 60 minutes, depending on the cell type) and produce a lot of cell clumps that were almost impossible to disaggregate. Trypsin and Accutase were found to work relatively well, but still produce a considerable amount of cell aggregates. This was mended by pipetting the cells up and down towards the end for the detachment incubation time and then leaving them for a bit longer than the usual protocol suggested (4 to 5 instead of 3 to 4 minutes). Using this additional procedure, Trypsin outperformed Accutase and was chosen as the standard detaching agent because of this reason, as well as the difference in price and the idea to have external receptors degraded being beneficial to the analysis. As the yield of single cells is crucial in this type of analysis, the amount of Trypsin applied was also slightly elevated compared to the original protocol (volumes listed in table 5 plus approx. 25%).

The tissue dissociated protocol was already optimised by collaborators at UKE Hamburg and thus taken as suggested.

10.2.2 Statistical encapsulation drops

Deterministic encapsulation [78] was reviewed and found to depend very strictly on the concentration of the cell suspension that was about to be encapsulated. Also, the design allowed encapsulation in 70 pL drops, which is about 5-10 times smaller than the ones produced with the statistical geometry and thus required very high cell concentrations in the suspension. Attempts to increase the droplet size and therefore decreasing the initial

cell concentration required resulted in the process becoming more stochastic, thereby losing its apparent advantage over the standard statistical encapsulation. Because of that, it was chosen to proceed using normal Poisson encapsulation (cf. section 6.3.1).

The chip design used for encapsulation featured cell injection module (cf. section 6.3.1), followed by a 100 um wide channel in which the substrate was injected from the side. Droplets were generated by flow focussing with a constriction width of 75 um. The height of the channels was 45 um, yielding slightly smaller droplets (300 instead of 660 pL) than the original cell encapsulation protocol [49].

As a cell suspension reservoir, a 5 mL syringe with a 6 mm stirrer were chosen with a stirring speed of 250 to 300 rpm, depending on the suspension volume (higher with increasing suspension volume in the syringe). The tubing chosen (HW30) had an inner diameter of 0.32 mm, which was found to yield less cell clumps compared to the one with an inner diameter of 0.59 mm (TW24). Suspension tubing was tried to be kept short (15 to 25 cm) and monotonously descend from the pump to the chip, avoiding the accumulation of cells in the tubing.

In the end, an oil flow rate of 4000 uL/h, a cell suspension flow rate of 750 uL/h, and a substrate flow rate of 250 uL/h were chosen. With these settings and at a cell concentration in the suspension of 2e6/mL, roughly one in four droplets was occupied with a cell. This lower concentration compared to the originally suggested one (cf. figure 10) had to advantage of lowering the ratio of droplets with two cells in them, therefore improving the accuracy at the cost of throughput, while still being able to profit from increased droplet stability.

10.2.3 Optimisation of droplet stability

Apart from the chip design and the decreased droplet size that already helped improve droplet stability, other parameters were varied as well in order to further limit the level of coalescence occurring within the emulsion. This was for the most part necessary because the cells were co-encapsulated with the MMP substrate, which was a peptide and thereby lead to substantial droplet destabilisation.

The originally suggested surfactant concentration of 0.5-1% [49] was increased to 2%, yielding a observable decrease in coalescence. The upper limit was found to be 2.5-3%, as the droplets tended to lose the cells afterwards if they were accelerated swiftly (*e.g.*, in the case of sorting). Incubation times were varied from 1 to 6 hours, and it was seen that after 4 hours the yield of intact emulsion decreased drastically. Two more factors that had an effect of droplet stability was the amount of emulsion collected (with less emulsion being more stable, probably due to diffusion from surfactant from the oil to the emulsion) and sudden temperature changes. Because the cells had to be incubated at $37°C$ and it was observed that even if the emulsion was stable at the point of taking it out of the incubator, it often degraded rapidly and almost fully. Therefore, the emulsion was chosen to be kept in an insulation box for heating up and cooling, enabling slow temperature changes and contributing to increased stability.

10.2.4 Optimisation of enzymatic readout

As already mentioned, one of the most striking destabilisers of the emulsion was the co-encapsulated substrate itself. Substrate concentrations of 2.5, 5, and 10 uM (final concentrations in droplet) were tested. It was found that 2.5 uM was not sufficient to distinguish between the HeLa and HT-1080 population after an incubation time of 3 hours or longer. An incubation time shorter than that was considered to be inadequate

because it would probably not detect MMP secretion as opposed to surface expression. A final concentration of 10 uM was already the cause of a largely coalescent sample in the otherwise same conditions. 5 uM showed sufficient separation of the signal coming from HeLa and HT-1080 cells for up to 4 hours (with 3 hours being slightly advantageous but also bearing more risk of missing secreted MMPs).

In the end, a substrate concentration of 20 uM in PBS was chosen that was diluted to 5 uM on chip with the substrate-suspension flow rate ratio of 1:4 as previously described.

10.3 Droplet sorting

The sorting chip consists of a 200 um channel where the droplets are reinjected and aligned after spacing and a constriction of 100 um while spacing. The height of the sorting device was chosen to be 45 um, the same as in the encapsulation device. For the spacing oil, a surfactant concentration of 0.1% PFPE-PEG and a flow rate of 1000 uL/h were chosen. The emulsion was reinjected at a rate of 20 uL/h. At the sorting junction, the default flow was diverted in the channel further away from the electrodes by applying a suction of 800 uL/h. This yielded between 5 and 15 droplets per second (subject to inaccuracies in pump speed), which could be sorted by aligning the laser spot to the middle of the channel and the inside of the downstream electrode and using the settings of 10 ms delay, 20 ms pulse duration, 14 kHz output frequency, and a minimum spacing of 50 ms.

With the flow rates mentioned, coalescent droplets that were split by the spacing oil were significantly larger than the original ones, enabling a clear distinction between coalescent and intact droplets. This is important to not falsely consider cells positive when they are part of a large coalescent blob.

10.4 Preparation of the primary cell sample

The goal of this single cell MMP activity screening was to determine whether or not there was indeed biological variation in the MMP secretion of cells in a primary tumour and, in contrast to the stromal cells, especially the cancer cells themselves. A patient tumour samples was collected at UKE Hamburg and digested with a collagenase/pronase mixture at $37°C$ for 3h. The sample was transferred to EMBL over night and then treated with Trypsin and washed for four times in order to eliminate extracellular receptors and possible ligands bindings to them. Cells were encapsulated in 350 pL drops of FreeStyle expression medium with a particle density of 3e6/mL, which corresponded roughly to 6e4 cells with a diameter of 10 um or above (flow rates: 4000 oil, 750 suspension, 250 MMP substrate in PBS; all units in uL/h). The emulsion was incubated for 4h at $37°C$ and the matrix metalloproteinase activity determined by the cleavage of a broad spectrum FRET peptide that was detected using 488/520 nm excitation/emission as in the cell line screenings before.

11 Results

11.1 In-bulk assays

11.1.1 Enzymatic assays

As mentioned in the experimental setup section, it was first needed to check whether the recombinant enzyme actually cleaves the fluorogenic peptide and the existing workstation setup was suitable for excitation and detection at the corresponding substrate wavelengths.

Results of the emission scan with 488 nm excitation wavelength of fully converted

substrate are shown in figure 17. Emission scans using the other available wave lengths (cf. workstation setup) did not show an increase in fluorescence in samples with the enzyme compared to the blank (results not shown). The sample including the enzyme constantly showed a 35-fold higher fluorescence compared to the blank for both PBS and DMEM at a range from 515 to 620 nm, peaking at 3400/5800 RFU at around 520 nm. This wavelength corresponds to the "green" PMT.

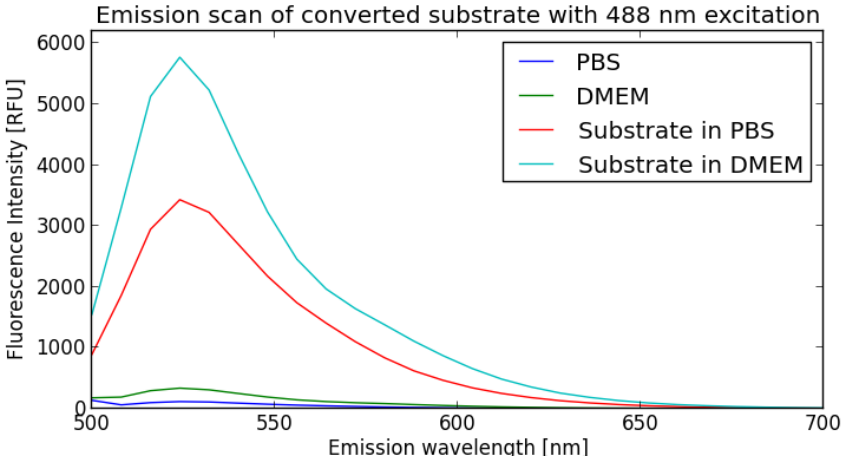

Figure 17: Emission scan of 5 uM 520 MMP FRET substrate XIV converted after five-hour incubation with 20 ng/mL rhMMP-1. Excitation wavelength 488 nm, gain set at 45. Excitation measurements taken with a bandwidth of 5 nm. It can be seen that the fluorescence maximum in both cases is between 515 and 530 nm with a high signal-to-noise ratio, which corresponds to the one of the available filters for the PMTs.

With the excitation wavelength fixed at 490 nm and the emission wavelength at 520 nm, the results of the kinetic measurement of substrate conversion by recombinant enzymes are shown in figure 18. Details of the experimental setup are described in section 10.1.1. It can be seen that for both PBS and DMEM, the samples with recombinant enzyme show a significantly higher fluorescence compared to the samples without the enzyme present. The blank with PBS showed almost no increase in fluorescence during the time of measurement and stayed around 480 RFU. The blank in DMEM showed 1300 RFU after 200 minutes. Comparing this to the PBS sample with 13000 RFU and a DMEM/FCS sample with 22000 RFU after the same time, it respectively yields 27-fold

and 17-fold increases at the end of measurement.

The linear regime of the sample curves during the measurement lasts from the beginning of measurements until about 80 minutes. At this time, the PBS sample showed a fluorescence level of 7500 and the DMEM sample one of 13000 RFU (with the blank at 480 and 750 RFU, respectively). This corresponds to a 16 and 17-fold increase.

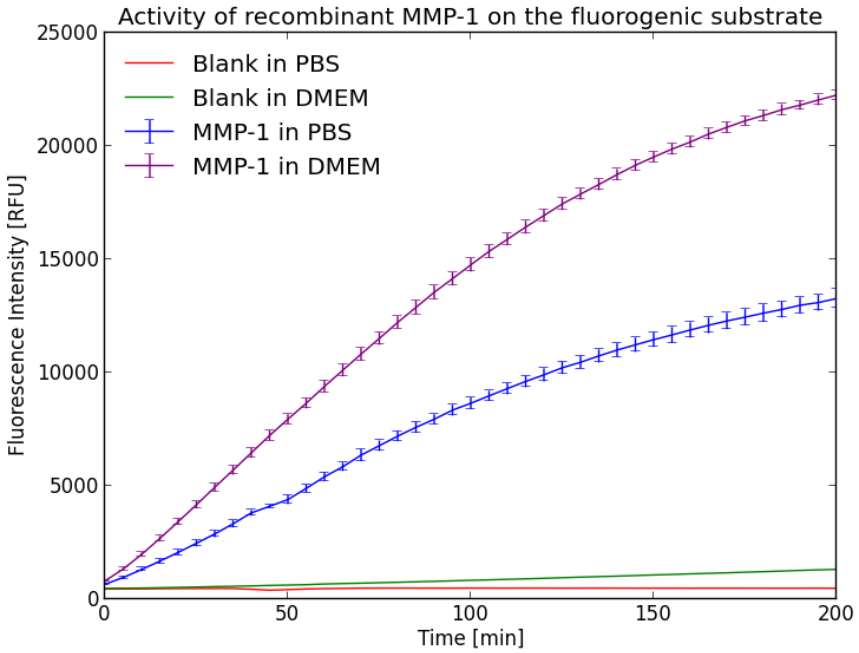

Figure 18: Results of the fluorescence by substrate conversion using recombinant MMP-1. Concentrations for substrate and enzyme were 5 uM and 20 ng/mL, respectively. Measurement in 5 minute intervals for a total of 200 minutes. Standard deviation shown for four replicates, blank measurements are the mean of two measurements. DMEM including 10% FCS.

11.1.2 Cellular assays

With the excitation and emission wavelengths chosen to be as close as possible to the existing workstation setup (cf. experimental setup), the results of the bulk kinetic activity assay using the HeLa and HT-1080 cell lines are shown in figure 19. The different media included PBS, PBS with 5% FCS, DMEM, DMEM with 10% FCS,

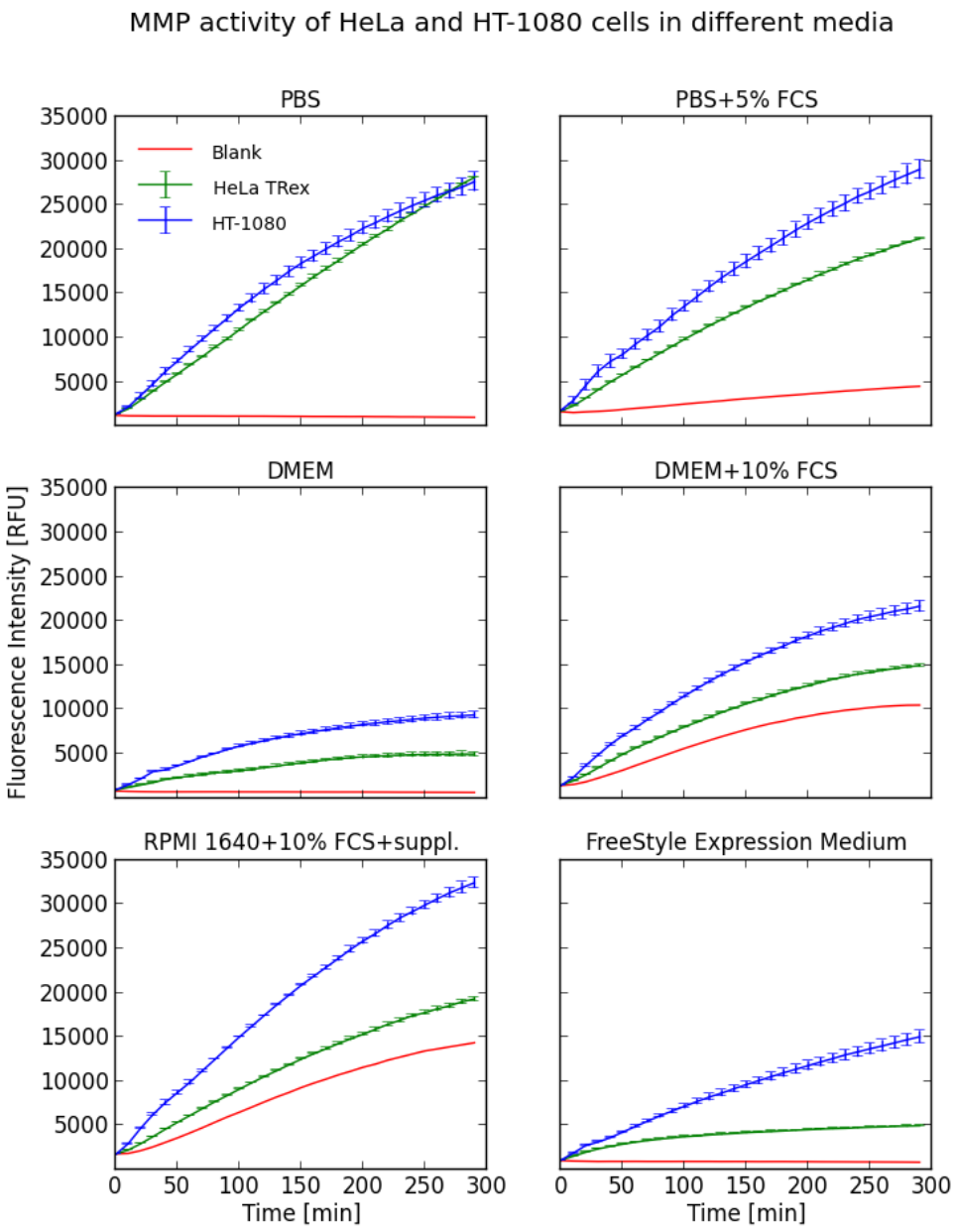

Figure 19: MMP activity of 22500 trypsinised HeLa and HT-1080 cells in different media with 1.875 uM substrate concentration. Standard deviation of cellular assays calculated from three replicates. For the blank, the mean from two measurements was taken.

RPMI with 10% FCS and supplements, and FreeStyle Expression medium.

The measurement was taken over a total time of 5 hours at an interval of 10 minutes. Cellular measurements included three replicates, the mean and standard deviation for which is shown in figure 19. For the blank, two replicates were measured and averaged with the range or standard deviation not shown.

The first property to notice is that the fluorescence readout of the different blanks (red lines) differ for different buffer or media. For PBS, DMEM, and FreeStyle Medium the fluorescence after five hours was still approximately the same as initially. For PBS with 5% FCS, the fluorescence increased to 4500 RFU at the end of measurement. For DMEM with 10% FCS and RPMI with 10% FCS and supplements, it increased to 10500 and 14000 RFU, respectively.

HT-1080 cells, which are known to exhibit MMP activity in the medium around them, always showed the highest activity in this essay (with the exception of PBS where they show the same activity as HeLa cells). The fluorescent readout ranges from 9500 RFU in DMEM over 15000 RFU in FreeStyle to 20000 RFU in DMEM with 10% FCS and 30000 in the rest of conditions.

HeLa cells exceed the blank fluorescent readout by about 5000 RFU compared to the blank in DMEM both with and without FCS, RPMI with 10% FCS, and FreeStyle Medium. In PBS they behave differently: without FCS they show the same amount of activity as the positive control, and with 5% FCS they reach about two thirds over the blank compared to HT-1080.

11.2 MMP activity in droplets

For the following results, a suspension of 2e6 cells/mL was encapsulated at a flow rate of 750 uL/h, 250 uL/h 6 uM substrate, and 4000 uL/h oil with 2% PFPE-PEG surfactant.

Incubation time was 4 hours. For details on the experimental setup, see section 10.2. Although the cells were counted before encapsulation to yield an approximate dilution, the real encapsulation densities are summarised in table 6.

Table 6: Droplet occupancy and cell distribution for the three encapsulations of HeLa cells, HT-1080 cells, and a 1:1 mixture of both. The cells were counted from a recording of the encapsulation for 1000 droplets each and the ratio calculated.

Cell count	HeLa [%]	HT-1080 [%]	HeLa and HT-1080 [%]
empty	90	86	83.5
1 cell	8.9	12.8	15.1
2 cells	0.9	1.2	1.3
3 cells	0.2	0	0
more	0	0	0

In order to understand what the diagrams represent, it is important to first introduce the concept of an isovolumic curve. Because the droplet is spherical (or if it is squeezed it at least has round edges) as well as for reasons of detection limitations, the fluorescent signal when a droplet passes the laser beam is not rectangular but bell-shaped. This means that droplets with lower fluorescence intensity tend to stay over the detection threshold for a shorter amount of time, *i.e.* that droplets with the same size but different fluorescence intensity appear to be different in size even though they are not (cf. figure 20).

The curve of fluorescence intensity readout from droplets in figure 21, reaching from 0 with a width of 0 to 0.4 with a width of 10 ms, etc. is such an isovolumic curve that is produced by this detection artefact. In figure 22 it is a bit less and in figure 23 a bit more pronounced, but the principle is the same: these are droplets with the same size, not different size as one could think when looking at the width values.

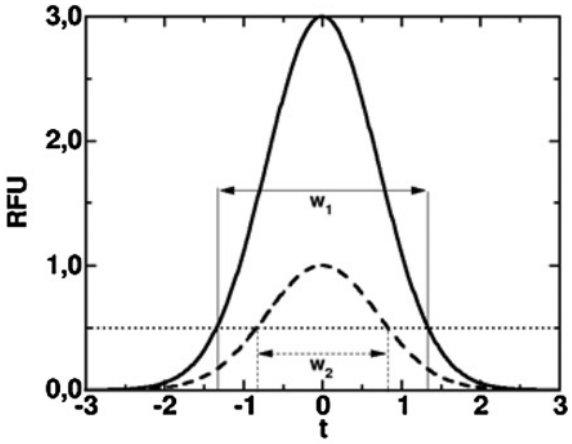

Figure 20: Influence of fluorescence intensity on apparent peak width with a set detection threshold. The droplets passing by are of the same size, yet the one with the weaker fluorescent signal appears to be smaller [49].

11.2.1 HeLa cells

From the encapsulated cells and empty droplets, the fluorescence level of a total of 25773 droplets exceeded the detection threshold for the HeLa cell screen. A coloured histogram of their intensity and how long it remained above detection threshold while passing the laser beam is shown in figure 21. One can see that the highest occurrence of matches was close to the origin of the diagram, meaning a low fluorescence readout for most of the droplets. From this starting point, there is a population in curved shape until a fluorescence intensity of about 0.6 RFU and a width of 10 ms. Another notable population enrichment occurs around the point of 0.3 RFU and 17 ms width. Apart from that there is a minor, more scattered population at around 0.1 RFU and a width of 12 ms, and some individual matches above 0.5 RFU and 12 ms width.

Starting from these populations, areas on the histogram have been assigned and the occurrence of matched droplets was counted in order to also provide a more quantitative measurements of the populations. The areas were designated $-$, $\pm$, $+$, and K with the readout they encompass as well as the total counts and relative occurrence summed

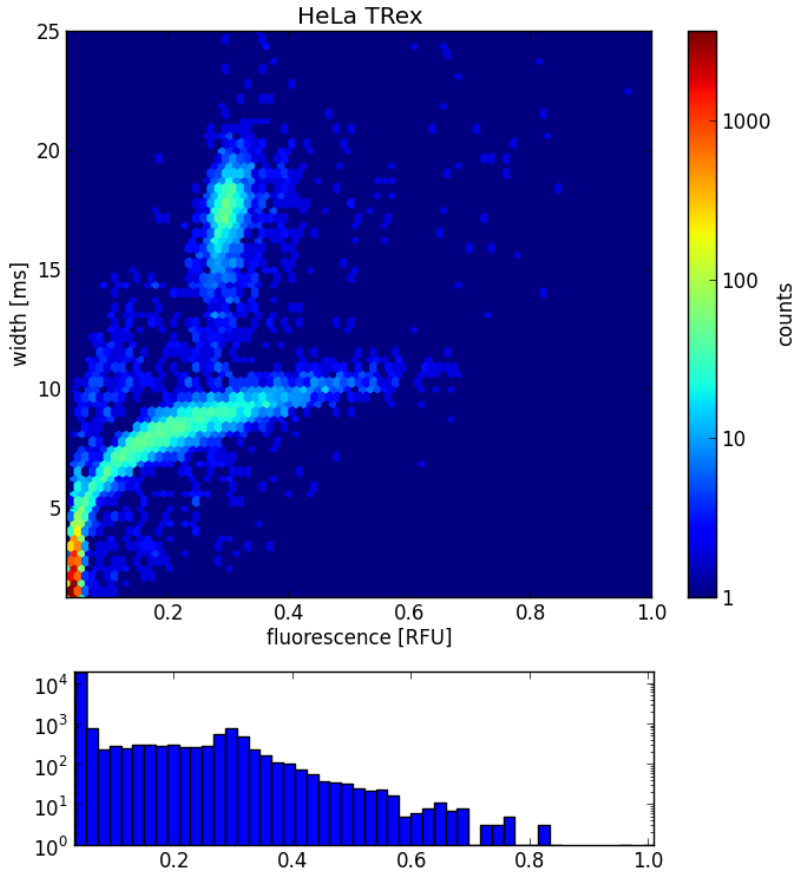

Figure 21: Screening result of 25773 droplets in part filled with HeLa T-REx cells. Fluorescence readout is shown in relative fluorescence units (RFU) on the x axis and the time the signal exceeded the threshold when a droplet passed the laser beam is shown on the y axis. occurrence of droplets with these distinct properties is indicated by colour coding on a logarithmic scale. The distribution of fluorescence is shown underneath using a histogram.

up in table 7. They were divided between matches below a width of 12 ms and a fluorescence intensity of 0.4 RFU, between 6 and 12 ms and 0.4 and 0.6 RFU, between 6 and 12 ms and above 0.6 RFU, and everything above 12 ms, respectively. There was a small remainder of droplet matches that was not accounted for by this scheme, which is also shown in the same table.

The vast majority of matches fell in the − category, with a total number of 23741 or 92.1% of total droplets that exceeded the detection threshold. 277 were assigned the

Table 7: Area designations for the droplet screening result of HeLa cells as shown in figure 21. Total count: 25773 droplets.

Designation	Width [ms]		Fluorescence [RFU]		Count	occurrence [%]
	minimum	maximum	minimum	maximum		
−		12		0.4	23741	92.1
±	6	12	0.4	0.6	277	1.1
+	6	12	0.6		20	0.08
K	12				1732	6.7
unassigned					3	0.01

category ±, which corresponds to 1.1% of all the droplets screened. In the + category, there are 20 droplets to be found, which corresponds to 0.08% overall. The designation K, marked by a higher width irrelevant of fluorescence intensity as assigned to 1732 droplets, or 6.7% total. 3 droplets, or 0.01% total were left unassigned.

11.2.2 HT-1080 cells

A total of 27670 droplets exceeded the detection threshold for the HT-1080 cell screen, a coloured histogram for which is shown in figure 22 with fluorescence intensity readout and droplet passing time above the detection threshold. As in the HeLa cell screen, the largest population can be found close to the origin, with a curve again protruding until a fluorescence level of 0.4 RFU and a width of 8 ms. A second major population can be found at 0.75 RFU and 11 ms width when following the curve's trend, with an intermediary decrease of the number of matching droplets between 0.4 and 0.6 RFU. A third major, more scattered population can be found with the centre at a fluorescence intensity level of 0.7 RFU and a width of about 20 ms. A second curve can be seen that leads up to this population, also starting from the origin. Apart from the large scattered population this curve is less pronounced than the lower one.

According to the population matches seen in the histogram, area designations have again been placed on the different readout values. The designation characters are the

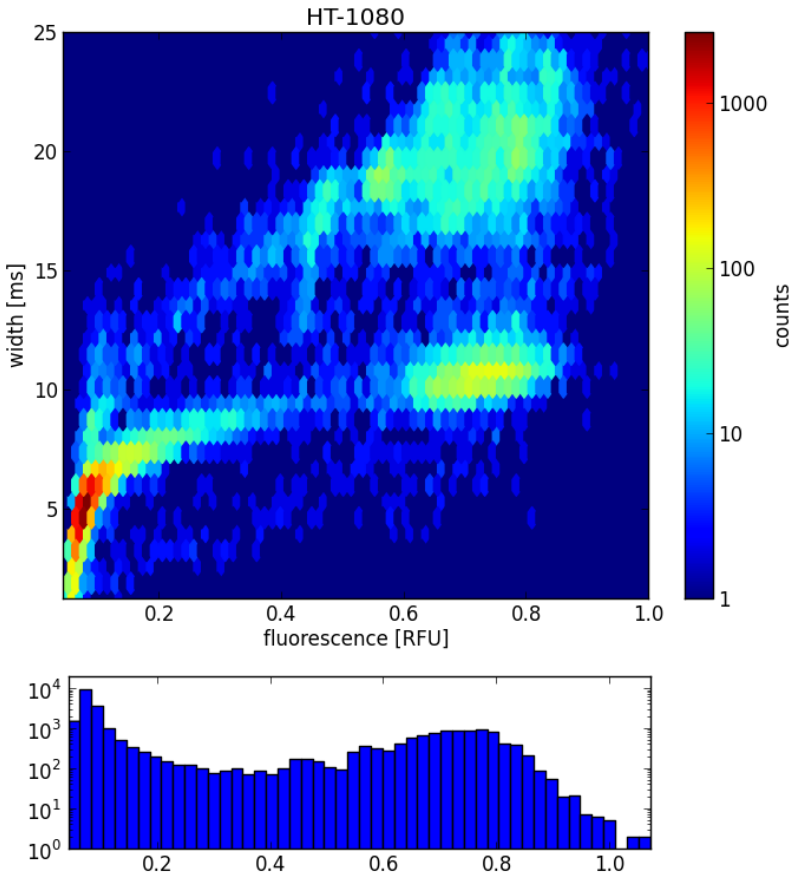

Figure 22: Screening result of 27670 droplets containing in part HT-1080 cells. Fluorescence readout in RFU vs. time the signal exceeded the detection threshold. Colours and histogram in logarithmic scale.

same as in the previous screen, namely $-$, $\pm$, $+$, and K. Which areas the encompass is shown in table 8, along with counts and relative occurrence.

The majority of droplets was again found within the boundaries of the $-$ category with a total number of 17244 matches or 62.3%. The $+$ population, found between a width of 7 and 13 ms with a fluorescence readout of about 0.6 RFU was founded by 3242 droplets or 11.7% of the total number screened. The intermediary population between these two, designated as $\pm$ had a total of 363 matches or 1.3%. The number of matches with the designation K, which were above a threshold of 14 ms width were higher than

Table 8: Area designations for the droplet screening result of HT-1080 cells as shown in figure 22. Total count: 27670 droplets.

Designation	Width [ms]		Fluorescence [RFU]		Count	occurrence [%]
	minimum	maximum	minimum	maximum		
$-$		10		0.4	17244	62.3
$\pm$	7	12	0.4	0.6	363	1.3
$+$	7	13	0.6		3242	11.7
K	14				6322	22.8
unassigned					499	1.8

in the previous screen, with 6322 droplets or 22.8%. 499 droplets, or 1.8% were left unassigned.

11.2.3 Mixed population

The results of the same screen already summed up in the previous two sections was also carried out with a population mixture, the coloured histogram for which is shown in figure 23. In total, 37877 droplets were detected and as in the previous screens and the biggest population can again be seen close to the origin, spanning a curve until 0.5 RFU and 7 ms width. As in the HT-1080 but in contrast to the HeLa cell screen, there is a second major population with the centre of 0.8 RFU and 8 ms width. This population is separated by a decrease of matching droplets around 0.5 to 0.6 RFU and 7.5 ms width. Another major population can be found at 0.7 RFU and 15 ms width, with an adjacent intermediary one at 0.5 RFU and equal width. There is a hint of a second curve starting at the origin and leading up to these two populations, albeit not very well visible.

The areas $-$, $\pm$, $+$, and K were designated as in the previous cases, with the boundaries summed up in table 9, again along with total number and relative occurrence. The $-$ category beneath a width of 10 ms and a fluorescent readout of 0.5 RFU again encompassed most of the droplets, with a total number of 19115 matches or 50.5%.

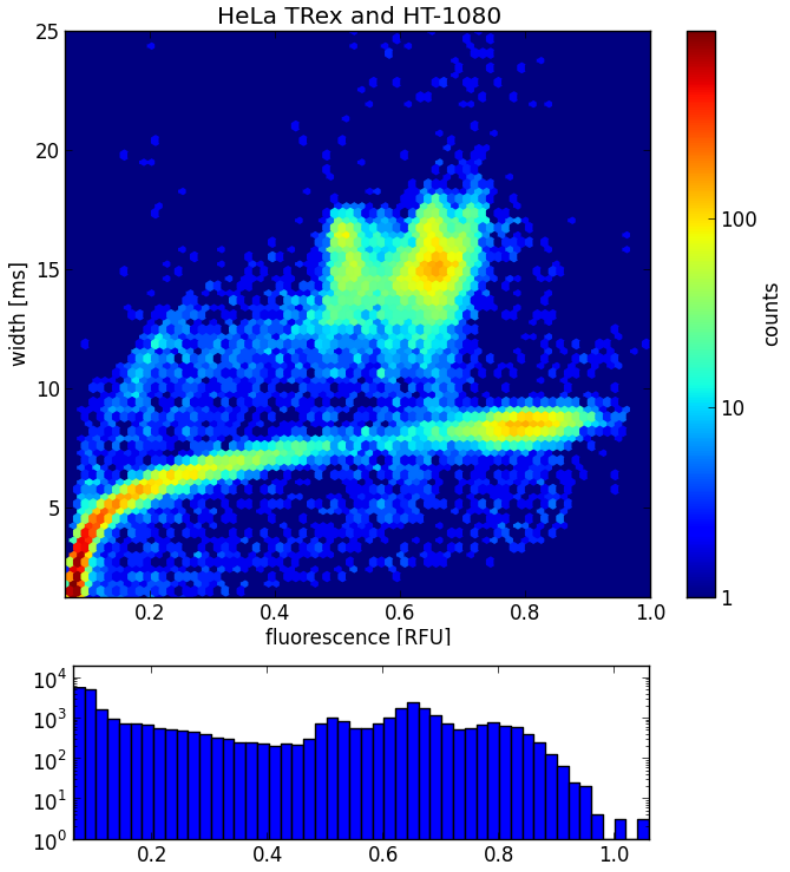

Figure 23: Screening result of a 1:1 mixture of HeLa T-REx and HT-1080 cells in 37877 droplets (not all filled), fluorescence readout in RFU vs. time the signal exceeded the detection threshold. Colours and histogram logarithmic scale.

The + category with a width between 6 and 10 ms and a fluorescence readout above 0.6 RFU had 5023 matching droplets or 13.3%. Intermediary matches designated the ± category contained 345 matches or 0.9%. The area code K with a width above 10 ms was assigned to 13080 droplets or 34.5% of the total number. 314 droplets or 0.8% were left unassigned.

Fluorescent images of the cell suspension that was used for encapsulation as well as the one that was positively sorted were taken using the fluorescence microscope and -camera

Table 9: Area designations for the droplet screening result of a mixture of HT-1080 HeLa cells as shown in figure 23. Total count: 37877 droplets.

Designation	Width [ms]		Fluorescence [RFU]		Count	occurrence [%]
	minimum	maximum	minimum	maximum		
−		10		0.5	19115	50.5
±	6	10	0.5	0.6	345	0.9
+	6	10	0.6		5023	13.3
K	10				13080	34.5
unassigned					314	0.8

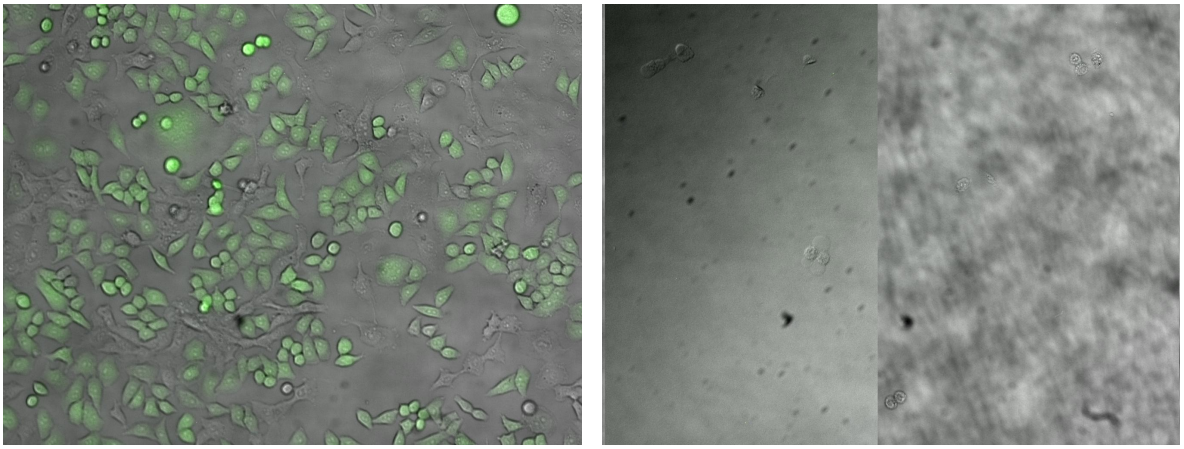

(a) Mixed population before sorting **(b)** Population after sorting

Figure 24: Tetracycline-induced GFP expression for HeLa T-REx (positive) and HT-1080 cells (negative) in a 1:1 mixture of both cell types before and strongly enriched HT-1080 population after sorting

and are shown in figure 24. Fluorescence corresponds to GFP expression that induced with tetracycline using the T-REx Flip-in system present in HeLa but not in HT-1080 cells. About half of the cells in the unsorted population, as shown in figure 24a, were fluorescence-positive, while the large majority of the positively sorted population was fluorescence-negative (figure 24b).

11.2.4 Primary tumour cells

Results of the fluorescence level and apparent width of the screened droplets containing primary cells are shown in figure 25. The largest population of droplets grouped by readout of the measured values of fluorescence intensity and duration was at 0.1 RFU and 15 ms. Two other relatively large populations can be seen at a fluorescence level of 0.3 to 0.4 RFU and a width of between 25 and 33 ms. Minor populations can be seen at 1.1 RFU and 22 ms width and the isovolumic curve leading to this point from the first population mentioned. In total, 16278 droplets were screened. Absolute fluorescence intensities between this screen and the previous ones may not be comparable due to a higher detection gain used (cf. discussion).

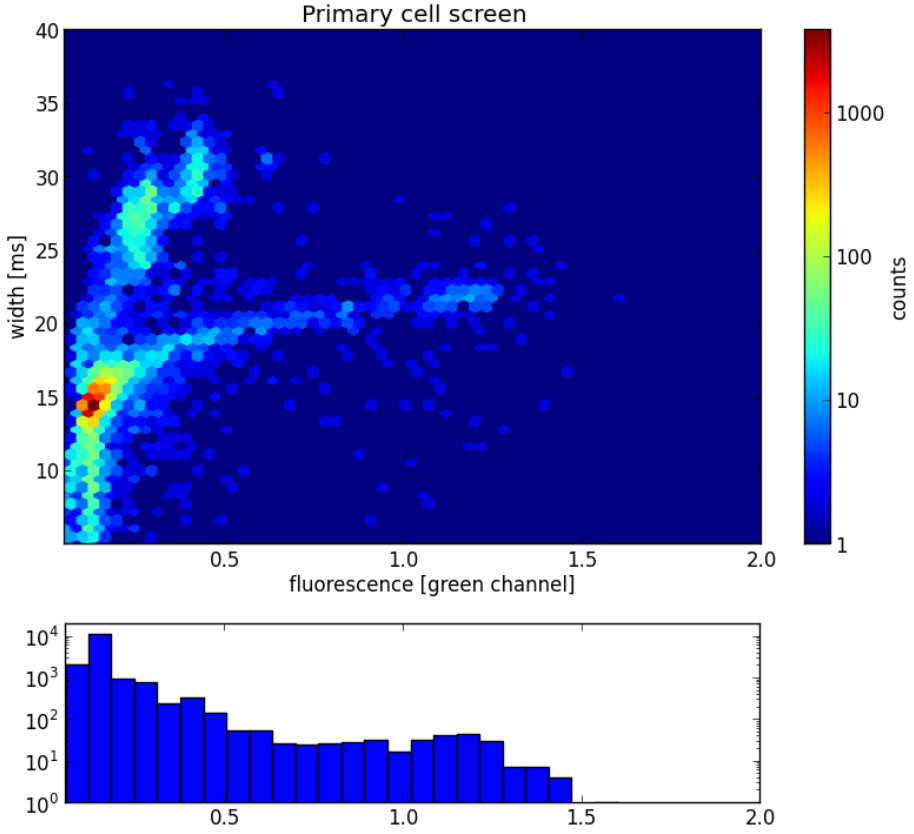

Figure 25: Screening result of single cell analysis of a primary prostate tumour sample

The resulting populations of the primary cell screen were designated the same symbols as with the previous screens using cell lines, summed up in table 10. The − area reached up to a fluorescence level of 0.5 and a width of 22 ms. Droplets assigned to the ± area had a fluorescence level of 0.5 to 0.65 and a width from 15 to 25 ms. Droplets assigned the + category had a fluorescence level above 0.65 while retaining the width requirements. The K category encompassed everything with a width above the previously defined categories.

Table 10: Area designations for the droplet screening result of the primary tissue sample disaggregated into single cells and encapsulated into a total of 16278 droplets. The corresponding screening results are shown in figure 25.

Designation	Width [ms]		Fluorescence [RFU]		Count	occurrence [%]
	minimum	maximum	minimum	maximum		
−		22		0.5	14477	88.9
±	15	25	0.5	0.65	92	0.56
+	15	25	0.65		281	1.7
K	22-25				1407	8.6
unassigned					21	0.13

12 Discussion

12.1 In-bulk assays

Ideally, one would always optimise a screening assay that one would like to conduct on the exact system it will run on later, which would be a microfluidic chip in this case. However, running assays on those takes a considerable amount of time and technical equipment, which means that the first steps of optimisations are better done in bulk.

12.1.1 Enzymatic assays

The emission scan (cf. figure 17) of the converted substrate excited at 490 nm showed a considerable level of fluorescence and a good signal-to-noise ratio in both PBS and DMEM w/ 10% FCS. This was in line with the available workstation setup using a 488 nm laser for excitation and a PMT that detected around 520 nm, which means that the substrate including the fluorophore and quencher could be used for screening.

The sample run in DMEM with 10% FCS showed a slightly higher background fluorescence than was present in the blank, which is negligible in this assay and both PBS and DMEM could be used for screening when looking for a high enzymatic activity as is the case when adding large amounts of recombinant enzyme.

The same can be said for the kinetic screen at the wavelengths where the fluorescence maximum occurs, *i.e.* a band around 520 nm (cf. figure 18). Again, both samples have a good absolute fluorescence intensity and a good signal-to-noise ratio from as little as 10 minutes into the screen until the end of measurement after 200 minutes.

12.1.2 Cellular assays

The goal of the subsequent microfluidic assay was to distinguish cells that actively show MMP activity under physiological conditions in the medium surrounding them from those that do not. HT-1080 cells are known to express membrane-bound MMPs. HeLa cells are known to produce MMPs intracellularly, but do not secrete them under normal conditions. This means that for the sake of this assay, HT-1080 cells are considered as positive and HeLa cells as negative samples, and it is important to be able to distinguish them from one another. An important difference of this screening compared to the one with recombinant MMP-1 is that the enzymatic activity is much lower and already approximates the cell- and substrate concentrations that will later be used when single

cells are encapsulated in droplets.

Looking at figure 18, a couple of trends can be recognised. For one, FCS concentrations, while negligible in the recombinant assay that showed high enzymatic activity compared to the cellular one, significantly influence the fluorescent readout of the blanks in a continuously increasing fashion with time. This leads to the conclusion that FCS has some proteolytic activity that competitively cleaves the MMP substrate. Low FCS concentrations like 5% show a basal level of activity, while 10% already shows significant substrate cleavage compared to the cell lines, leading to a worse signal-to-noise ratio in the samples where more FCS was added, *i.e.* DMEM and RPMI (middle right and bottom left, respectively).

PBS with 5% FCS shows a smaller fluorescent intensity of the blank, but since it is a buffer and not a medium might stress the HeLa cells to extracellularly produce MMPs that almost reach the level of activity of the positive control HT-1080, leading to a unfavourable ratio between the positive and the negative sample. Adding even more stress to the system by completely leaving out serum and thereby possibly triggering a starvation response in HeLa cells that makes them produce and secrete even more MMPs, in this case *en par* with the positive control. In any case, PBS buffer is thus not suitable as a screening medium.

The two media left are DMEM without FCS and FreeStyle Expression Medium. Both show an excellent signal-to-noise ratio, yet neither has the same absolute intensity of fluorescence compared to RPMI with FCS or PBS. The absolute intensity of DMEM is even lower, and the ratio of positive and negative cell line is only about two to one. This also eliminates DMEM as possible screening medium, leaving only FreeStyle.

The absolute level of fluorescence reached from MMP activity in FreeStyle Medium is approximately half of the maximum activity seen, which was still considered as suitable.

The ratio of the positive HT-1080 cells compared to the negative HeLa cells was three to one, which was also considered enough difference to likely be able to obtain two distinct populations in the microfluidic screening process. The signal-to-noise ratio of the HT-1080 and HeLa cell populations over the blank were 6 and 18, respectively.

12.2 MMP activity in droplets

The microfluidic screen of single cells in droplet microcompartments and sorting of the latter is a technically challenging task and the system is relatively new, which coincides with a lot of aspects not being completely optimised. On the other hand, there is the possibility of using fluorescence-activated cell sorting, a technique which was been widely used in many laboratories and is known to work well. There is, however, one crucial advantage of using droplet-based microfluidics compared to FACS sorting: the latter can only screen for the staining of epitopes, and not for the actual enzymatic activity implemented by a cell. The activity-based screens that droplet-based microfluidics enables are therefore able to answer slightly different biological questions at single cell resolution that could not have been investigated before, including the characterisation and quantification of secreted molecules.

The other competing technology that does enable activity-based single cell screening are *e.g.* 1536-well based robotic systems that operate in very small volumes. However, they are not able to reach either the throughput that droplet-based microfluidics allows for, neither the extremely small sub-nanoliter volumes that can be reached for screening and thus also detect very low enzymatic activity.

12.2.1 HeLa cells

The most striking feature of the HeLa cell screen result shown in figure 21 is that there is no population that is positive for activity on the MMP substrate. In total, there are 20 droplets, or 0.08% of the total number screened that fell into this category - a number that is almost negligible. The droplets that showed activity on the MMP substrate most likely contained MMPs, but it can not be excluded that some other protein has activity on the substrate as well. For instance, in the bulk assays, FCS has been shown to has some substrate cleaving activity too. However, it is very well possible that some HeLa cells indeed secrete MMPs, as they showed a positive stain for MMP-12 that is located intracellularly (as did the HT-1080 cell line; results not shown).

Droplets found in the area K, which are coalescent and were thus excluded from further analysis, encompassed 6.7% of the total number screened. This is in line with the coalescence numbers previously reported for cell encapsulation [49].

The bulk of the droplet population was stretched out between the $-$ and $\pm$ areas, which corresponds to empty droplets and those containing cells (as confirmed by recording the detection process and observing cells in droplets then assigned to either area). The extent of the stretch of the population from 0 to 0.5 RFU leads to the conclusion that there is some sort of basal MMP activity that HeLa cells exert on their surrounding medium and not only produce them intracellularly as shown by the MMP-12 stain. The stretch indicates this effect being relatively varied among the cells.

Cells assigned to the $-$, $\pm$, and $+$ categories corresponded to non-coalescent droplets that we can assume to have the same distribution of cells as determined by analysing 1000 droplets upon encapsulation (cf. table 6). We can also assume that the droplets that contained cells always had an equal or higher fluorescence compared to the droplets

that did not contain cells (an assumption verified by analysing the cell content and fluorescence level of droplets in the video recording of the sorting process). Using these properties, we can determine the average level of fluorescence for empty and filled droplets. Those were put at 0.005 RFU for empty droplets and 0.25 RFU for those containing HeLa cells, which corresponds well to the observed difference between HeLa and HT-1080 cells in bulk (cf. figure 19) and in droplets (figures 21 and 22 for HeLa and HT-1080 cells, respectively). The signal-to-noise ratio between the empty droplet and HeLa average is 1:50, which is an improvement of almost ten times compared to the bulk results. However, due to measuring single cells instead of the population average, the fluorescence readouts still overlap.

12.2.2 HT-1080 cells

Compared to the cell screening procedure that looked only on HeLa cells, the one conducted with only HT-1080 shows a different picture. Here, the populations between the empty droplets and those containing positive cells are clearly distinct. Another difference is that the amount of coalescent droplets is larger, which may either be to an inherent property of the HT-1080 cells (*i.e.*, they secrete a compound that destabilises the droplets) or caused by enzyme cleavage of the substrate that leads to more wetting by counteracting the surfactant.

When excluding the coalescent population from further analysis, one can calculate that the number of positive droplets and the number of negative droplets correspond to the ratios that were predicted by the ratio of occupied droplets compared to those which did not contain cells (cf. table 6). This way, one can conclude that almost the whole population of HT-1080 cells produces and secretes MMPs and those were the droplets assigned to the + category. This is in line with the large majority of the droplets containing cells being fluorescence positive in the video recording.

The reasons why the populations and gates are relatively but not entirely concordant between the different screenings is that even though the same chip was flushed and used again, thereby discarding all debris that might have been left on chip and still maintaining the exact same channel geometry as well as PDMS height, is that the laser spot might have not been aligned to the exact same position, causing slight differences in the apparent droplet width and fluorescence intensity.

12.2.3 Mixed population

The results seen for the screening and detection of droplets containing the 1:1 mixture of HT-1080 and HeLa cells (figure 23) is almost an overlay of the screening experiments conducted by the two cell lines separately (figures 21 and 22). The fluorescence intensities of the population averages of the distinct droplet populations corresponding to HeLa and HT-1080 cells both agree with the bulk measurements, where the HeLa population showed a fluorescence level of 0.1 to 0.5 RFU and the HT-1080 population a fluorescence level of 0.6 to 1.0 RFU. The exact numbers of RFU can not be compared to the previous experiments because a higher detection gain was used. However, the ratios still hold true.

In this case the mixing of populations allowed to determine not only the separability of the two cell types by means of detection but also by means of using a microfluidic droplet sorter to selectively target droplets with a high fluorescence readout and extract them. The emulsion containing only positive cells can be broken with PFO afterwards and the cells recultivated. The unsorted population mixture was expected to yield about 50% of GFP-fluorescent cells corresponding to the HeLa cell type, while the non-fluorescent ones were HT-1080 cells. This is in agreement with figure 24a. Cells recovered after sorting were also recultivated, however, due to their low number and the surface area of a 96 well plate only a representative fraction of the re-isolated cells is shown in figure

24b. Fluorescence-positive cells were also found in the sorted population, but with a frequency of about 1 in 100, corresponding to a 50-fold enrichment.

12.2.4 Primary tumour cells

Biological variation in MMP activity between the encapsulated cells was observed with a positive-negative ratio of about 1 to 20-50. The screening result is shown in figure 25. The estimate of the ratio between positive and negative cells is broad because it was not always possible to observe cells on the video recording of the sorting process when PMT detection is performed in parallel and the microscope lighting needs to be band-filtered and dimmed, requiring higher shutter times for the camera and thus more blur in the acquired images.

Cells considered to be MMP positive showed highly variable activity among themselves, with only a slight population enrichment in the + area. 250 positively sorted cells as well as an unsorted sample were frozen for further analysis using antibody stainings and/or sequencing in order to determine whether the MMP-positive cells are indeed cancerous. The low number of cells that showed a positive screening result also highlights one of the crucial differences between the screening of cells originating from a cell line and those originating from an actual patient: while the former are virtually unlimited, the amount one can attain from the latter is. With a total availability of 150,000 particles, 7500 of which were the size of HeLa cells and the rest likely some undigestible tissue components, they were encapsulated in droplets 16,000 of which maintained their original state and could be screened for activity.

While this result is generally encouraging, there are a couple of steps that need to be taken by a follow-up project that will employ the determined experimental procedures and conditions that have been shown to work reasonably well. For instance, the pos-

itively sorted cells still need to be confirmed to be cancer cells, which can be done by staining for upregulation of c-myc or Erg, or loss of PTEN that are frequently reported in prostate cancer [39] and where at least one should be the case in the majority of samples. Also, the disaggregation procedure could be further optimised to yield a higher number of single cells in order for a total yield of positive ones to reach about 1000 which would enable a decent library generation for sequencing without the need for extensive whole genome amplification.

13 Conclusions

13.1 Technological

To conclude the experiments carried out, the microfluidic technology was found to be a viable platform for single cell screening for the enzymatic activity of secreted and membrane-bound proteins. However, while the technique of continuous flow microfluidics has advanced to a level that it can routinely compete with other types of assays, droplet-based microfluidics still requires a lot of assay-tailored optimisation for all parameters used. Droplet coalescence is still a major issue when high concentrations of peptides (in the range of uM) are present in the droplets.

Remembering these issues, it is important to also consider the potency of the technology to do droplet-based screening. An emulsion of 100 uL can at least hold 500,000 distinct bioreactors (assuming each has a volume of 500 nL and half of the volume present in an emulsion is made up of the aqueous droplet phase, which is rather conservative) that, taking the stochastic nature of particle encapsulation into account, can be filled with 150,000 distinct biological samples. This represents a number-to-volume ratio that can not be reached with any other technique to date In this work, the cell densities

were kept a bit under the theoretical limit of 30% of droplets being filled with single cells in order to aid the overall emulsion stability that was severely compromised by encapsulating the fluorescent peptide with the cells to begin with (cf. table 6).

Overall, the issues mentioned could be mended with either decreasing the droplet size further, using another surfactant that has been reported to be more stable while still being biocompatible [49], or encapsulate only the cells in their respective microreactors and fuse the substrate to each individual droplet later on [67]. Given those possibilities for further improvement, the technology of droplet-based microfluidics shows promise in both biochemical analysis of single cells as well as a variety of other applications summarised in sections 3.1 and part IV.

13.2 Biological

With the experiments conducted, it has been shown that droplet-based microfluidics can be used to distinguish between single cells of a cell line that secretes MMPs and one that does not, and that these populations can be successfully separated on the basis of this phenotype. Cells of a primary tumour sample of a prostate carcinoma has been shown to exhibit a certain variety in MMP secretion, with 1 in about 20 to 50 cells being MMP-positive.

What is still left to do is estimate how many of the positively sorted cells are indeed cancer cells, as opposed to immune cells and other cell types that are known to exhibit this phenotype. Since the screened prostate tissue sample was from a tumour that was operatively removed, we can assume that the content of cancer cells will be relatively high, and the content of MMP-secreting cancer cells alike.

Once this is confirmed, DNA can be isolated from the samples and given to whole-genome sequencing. The coverage that can be reached will be determined by how

many cells or how many nanograms of DNA will be there in the end, but we are optimistic that this can be done with none or a relatively low amount of whole genome amplification before sequencing, the application of which would introduce a sequencing bias that is undesirable.

To conclude, we expect to find genetic determinants of cancer cells that mediate MMP expression and -secretion. While a little is known about the transformation from a non-MMP-secreting phenotype to one that does, we may well find novel determinants that have not been described before. Those could serve as hints for targeted drug development that ultimately tries to inhibit MMP signalling exclusively in cancer without interfering with the physiological processes.

Part IV

Outlook: Microfluidic applications in Biotechnology

With the decrease in volume that microfluidics enables to run biochemical assays on and the accompanying decrease in the chemicals used up in the process, the costly process of drug screening is also one that has been suggested to be optimised by lab-on-a-chip technologies. For instance, the Mountain View (California, US) based company Caliper Technologies demonstrated that it could screen 750,000 compounds in a drug library against a protein target consuming only 750 ng of the latter in the process, corresponding to 1,000,000 compounds per ug of target protein. Comparing to batch-based approaches, the system operates with 100 times less protein at a 10 times shorter time scale [80].

However, the general approach of miniaturisation in a biotechnological context is not only applicable for drug screening, but also other research topics that can make use of small volumes. Decreasing the size of assays has proven to enable analyses of cellular systems down to a single mammalian, yeast, or even bacterial cell [49]. Although most of the effort has been focussed on detection so far [81], there are some approaches that took microfluidics to establish cell- or protein based biochemical production systems [82, 83].

14 Assay and bioreactor miniaturisation

14.1 Microscale reactors with immobilised enzymes

One of the obvious advantages when using a microfluidic system as a bioreactor to carry out reactions using, for instance, immobilised enzymes is that the same amount of liquid is exposed to a larger surface area [84]. This has the potential to increase reaction speeds while retaining a structural control that might not be achieved by using a porous carrier material in a macroscale fermenter. While the approach of using microfluidic channels as bioreactors for reactions carried out by immobilised enzymes is still in its infancy [85], they have been shown to outperform batch-wise operations in terms of both process optimisation as well as actual reaction speed, the latter because of favourable mass and heat transfer characteristics [85, 86, 87, 88, 89]. Another advantage that has been suggested is a possible scale-up due to massive parallelisation of available modules instead of increasing the reactor volume, thereby retaining all characteristics testable on a small scale and reducing the need for further optimisation [84]. However, despite the advantages the microfluidic technology promises, there has been no exhaustive study quantifying those and comparing them to the classical methods.

14.1.1 Immobilisation using the streptavidin-avidin system

Mao *et al.* [83] used streptavidin-conjugated alkaline phosphatase and horseradish peroxidase, and avidin-conjugated glucose oxidase that they immobilised using on-chip functional biotin groups after treatment of PDMS with 3-mercaptopropyl trimethoxysilane and N-y-maleimidobutyryloxy succinimide ester (GMBS). On-chip dilutions of the substrate combined with the laminar flow characteristics present on microscale fluid systems allowed an advanced analysis of enzyme kinetics in a single experiment. The au-

thors also constructed a glucose biosensor, immobilising glucose oxidase and horseradish peroxidase in a subsequent manner [83].

14.1.2 Immobilisation using glutardialdehyde

Thomsen *et al.* [82] developed an alternative immobilisation method using silanisation and glutardialdehyde treatment on PDMS channel with CelB from *Pyrococcus furiosus* as a model system. Their chip consisted of eight parallel channels with a width and height of 350 um and 250 um, and a length of 64 mm, respectively, yielding a total reactor volume of 167 uL. For better mixing, passive elements to increase the turbulence were added every 2.5 mm. This surface area allowed for 56 ug of protein to be covalently attached to it (cf. figure 26).

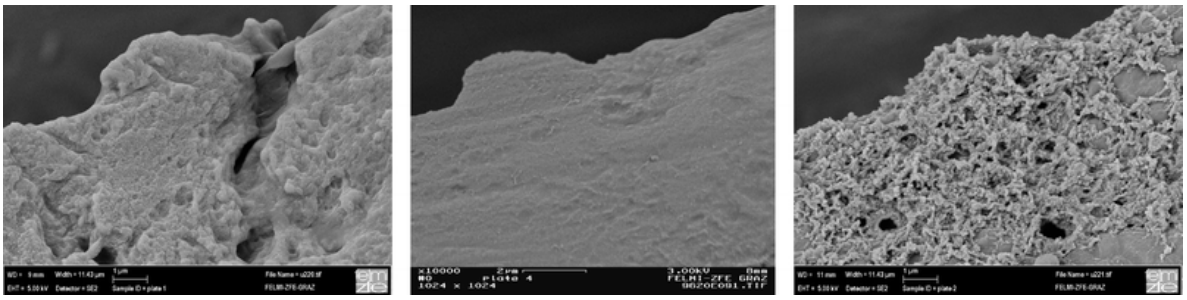

Figure 26: Electron micrographs of untreated PDMS surface (left), after silanisation and treatment with glutardialdehyde (middle), and with covalently lined enzyme (right) [82]

The setup was used to synthesise beta-glucosylglycerol using 2-nitrophenyl-b-D-glucoside (oNPGlc) as a glycosyl donor substrate and glycerol as acceptor [90]. It did, however, not show a substantially enhanced transglycosylation rate as Kanno *et al.* previously found [90, 88].

14.2 Inhibitor design and drug efficacy testing

Although microfluidics can be used for combinatorial synthesis of compounds [91, 92], most of the research was focussed on analytical applications [51]. One of the latter are cell-based assays that quantify the effect of stimuli on the cells by fluorescent readout. A stimulus can for instance be an enzyme inhibiting drug or a ligand that docks to a receptor and activates a signalling pathway.

In this case, usually multiple assays are run with different concentrations of the active compound to determine a range in which it can be used effectively. Ye *et al.* [62] developed a microfluidic module to ease this process by using inlets for medium and drug compound and generating a gradient thereof on the chip itself, running multiple experiments at once. Figure 27 shows a schematic of such an integrated chip using a gradient generator and downstream cell culture chambers that are exposed to different drug concentrations. Fluorescence again functions as quantitative readout of the response to the stimuli the cells are subjected to. Using this chip design, experiments that would otherwise have needed to be conducted in 64 individual chambers can thus be performed on one chip.

Another feature of using flow cells for cell culture is that the concentrations of the active compounds are constant over time, as they are constantly exchanged with the medium. This way, cells have been found to respond to tumour necrosis factor alpha (TNF-alpha) in a digital fashion: the concentration of the signal does not correspond how active cells are, just which fraction of the population switches to an active state. Another possibility when using not a gradient generator but chip valves is to subject the cells to different stimuli at different times, or to apply a burst of compound on demand and see how their reaction develops over time [63], providing an alternative to developing working fusion proteins between photoreceptors and intracellular signalling

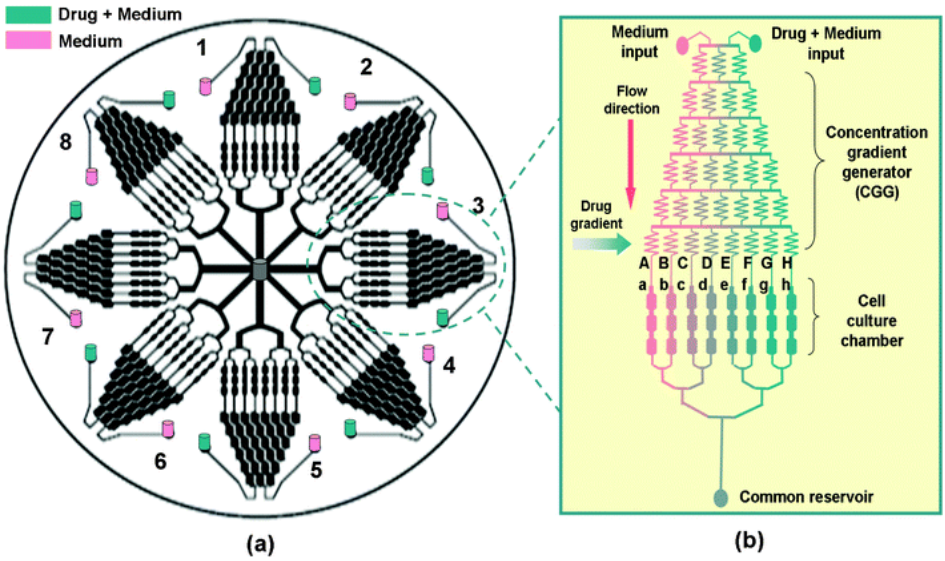

Figure 27: Schematic of an integrated chip for cell-based high content screening. The device consists of eight subunits, each comprising a gradient generator with medium or medium and drug input, followed by parallel cell culture chambers and leading to a combined waste outlet [62].

domains as is used for optogenetics.

15 High throughput using droplets

As already mentioned in section 3, one compelling reason to consider microfluidics platforms, especially droplet-based microfluidics, is the high throughput in sample generation and processing that can be reached by using small chambers or droplets as individual microcompartments. This also holds true for biotechnological applications. However, while the technology seems promising and there have been numerous proof-of-principle studies, the platform is far from being mature and biological problems are just beginning to be tackled with it.

15.1 Activity-based single cell screening

An obvious application of using picoliter volumes in screening assays is that the concentrations reached when investigating the behaviour of a single mammalian, yeast, or even bacterial cell can already be measured, thereby lifting the requirement to rely on population averages otherwise. The thesis project is an example of such a screening procedure for biomedical applications, but the analogous approach can be used for screening of a cell population heterologously expressing, for instance, different enzyme variants without the need for signal amplification by *e.g.* colony formation of this cell.

Such a hypothetical project could include a pool of gene variants being produced by mutagenic PCR and homologously recombined into *Pichia pastoris*, or the ectopic integration of one or more gene variants with unknown physiological consequences. In case of the former, the cells obtained a similar but slightly different copy of a gene that they express and secrete (possibly using a gene fusion with an alpha factor). These cells could be encapsulated into distinct droplets, incubated until they secreted enough protein, and then screened using a reaction with a fluorescent readout. The obtained positive clones could then be sequenced or subjected to other analyses.

One hot research topic of determining the protein activity secreted by single cells is antibody screening [68, 69, 67], one reason for which is that the diversity of the secreted proteins does not have to be introduced in the cell population but is intrinsically present. For instance, in an experiment conducted by El Debs *et al.* [67], the antibodies of two different hybridoma cell lines that are known to express antibodies inhibiting and not inhibiting the ACE-1 enzyme were screened for their functional inhibition. In order to do this, both were encapsulated in droplets containing the enzyme and incubated until they secreted a sufficient abundance of antibody to influence the activity thereof. After this time, the droplets were fused to droplets containing a fluorogenic ACE-1 substrate,

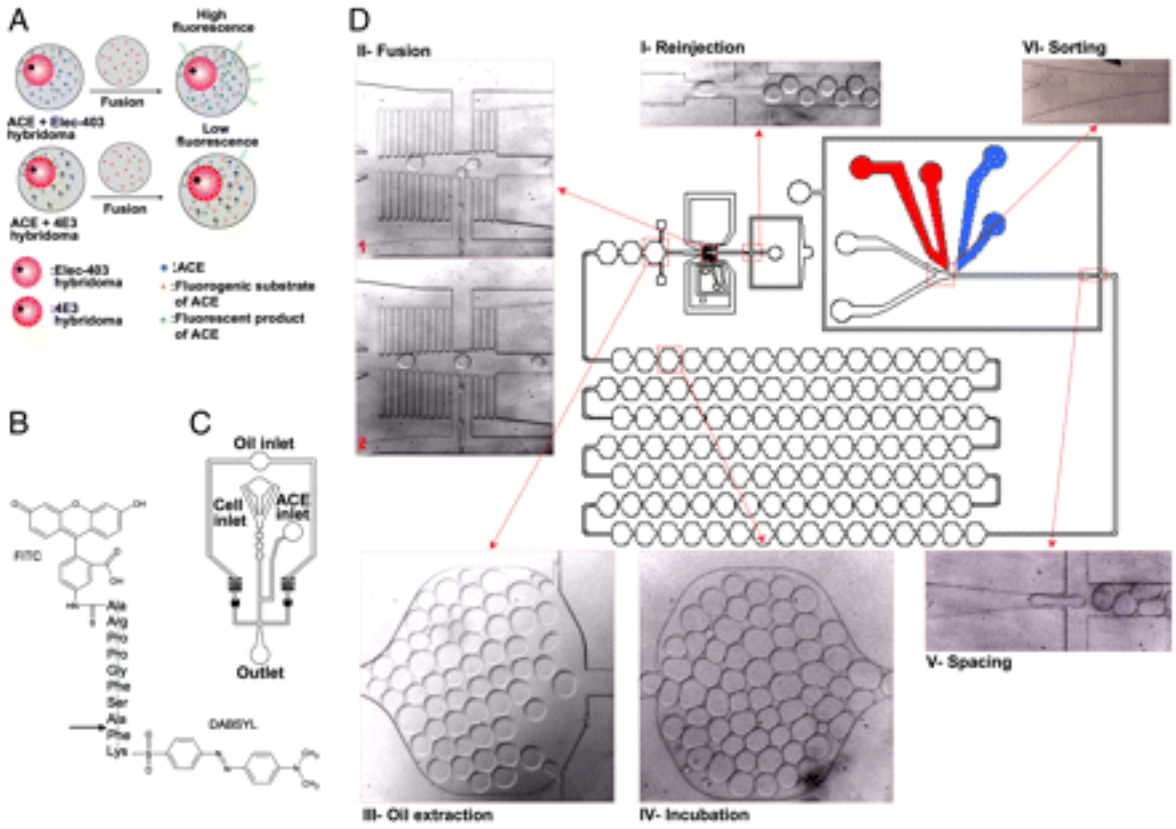

Figure 28: Schematic of experiments and microfluidic setup. (A) Hybridoma cells either expressing the ACE-1 inhibiting antibody 4E3 or the allosterically binding analogue Elec-403 are encapsulated with the enzyme and after an incubation time of six hours off-chip fused to a droplet containing the fluorogenic substrate. Lower fluorescence corresponds to enzyme that was inhibited by the antibody. (B) Structure of the fluorogenic substrate for ACE-1 with an arrow indicating the cleavage site. (C) Microfluidic design for cell encapsulation, the same as used in the thesis project. (D) Microfluidic design of the integrated chip containing a fusion and sorting module separated by a delay line [67].

kept in a teardrop-shaped delay line, and their fluorescence level was subsequently measured. This did not only serve as a proof of principle for inhibiting antibody binding assays, but also showed a larger than thought variety within a distinct cell line. A schematic of the screen conducted is shown in figure 28.

15.2 In-vitro directed evolution

Droplet-based microfluidics has also been used to create a system for directed evolution that runs entirely in vitro, an approach that is hardly possible using classical techniques due to the concentration of reagents required and the number of samples needing to be processed [70, 71]. In this case, single molecules of a gene encoding a protein with a desired function were encapsulated in droplets that served as reaction microcompartments, similar to the project described in this thesis. Alongside those genes, all the required reagents for a PCR were added as well, and the emulsion was thermocycled like a standard PCR reaction mix. Coalescent droplets were removed on-chip using passive size sorting and the droplets with the right size fused to other droplets containing a cell-free transcription-translation (IVTT) mix including the substrate for the reaction the protein catalyses. This mixture was taken off-chip and incubated in order for translation to occur. Thus, this process started with droplets in which single DNA molecules were encapsulated and ended with the same droplets containing not only 30,000 copies of that gene, but also the protein that was used for an activity-based fluorescence screen afterwards [70].

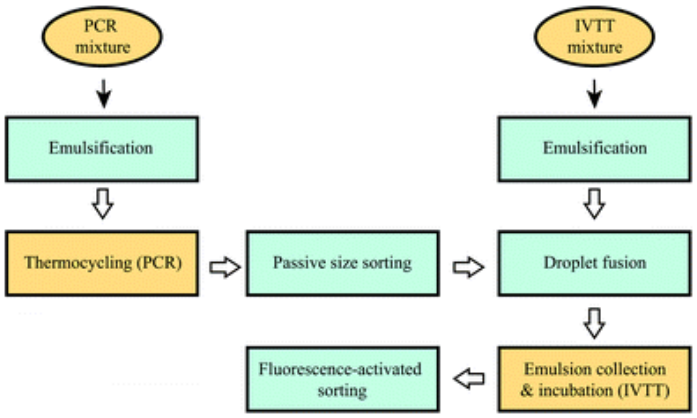

Figure 29: Schema of the directed evolution experiment. Steps that were performed on-chip are coloured blue, the ones that were performed off-chip yellow [70].

Fallah-Araghi *et al.* [70] used this system (cf. figure 29) to isolate *lacZ* from *lacZmut*

genes, the latter of which had a frame shift that both disrupts the beta-galactosidase domain as well as removes an internal *Sac*I restriction site [93]. The assay concentration of the *lacZmut* gene ranged from the same as *lacZ* to 100 times more concentrated, with FDG (Fluorescein di-b-D-galactopyranoside) used as a substrate that fluoresces once cleaved. Fluorescent readout was measured with a laser/PMT setup, indicating high enzyme activity. Positive droplets were fused to a continuous aqueous stream using electrocoalescence and the product verified with *Sac*I digestion after PCR amplification [70].

However, while the experiment was successful in a proof-of-principle run, the authors did not run an actual directed evolution experiment on their setup proving that the system can indeed be used for multiple rounds of amplification until improvements in enzymatic activity can be seen. The enzymatic activity shown in this case is always the one between negative and positive control, which will be far more easily distinguishable than slow and gradual improvements therein.

Part V

Literature

References

[1] Douglas Hanahan and Robert A. Weinberg. Hallmarks of cancer: The next generation. *Cell*, 144(5):646–674, March 2011.

[2] Douglas Hanahan and Lisa M. Coussens. Accessories to the crime: Functions of cells recruited to the tumor microenvironment. *Cancer Cell*, 21(3):309–322, March 2012.

[3] Douglas Hanahan and Robert Weinberg. The hallmarks of cancer. *Cell*, 100(1):57–70, January 2000.

[4] Mark A. Lemmon and Joseph Schlessinger. Cell signaling by receptor-tyrosine kinases. *Cell*, 141(7):1117–1134, June 2010.

[5] Esther Witsch, Michael Sela, and Yosef Yarden. Roles for growth factors in cancer progression. *Physiology*, 25(2):85–101, April 2010.

[6] Nikki Cheng, Anna Chytil, Yu Shyr, Alison Joly, and Harold L. Moses. Transforming growth factor beta Signaling–Deficient fibroblasts enhance hepatocyte growth factor signaling in mammary carcinoma cells to promote scattering and invasion. *Molecular Cancer Research*, 6(10):1521–1533, October 2008.

[7] Neil A. Bhowmick, Eric G. Neilson, and Harold L. Moses. Stromal fibroblasts in cancer initiation and progression. *Nature*, 432(7015):332–337, November 2004.

[8] Deborah L. Burkhart and Julien Sage. Cellular mechanisms of tumour suppression by the retinoblastoma gene. *Nature Reviews Cancer*, 8(9):671–682, September 2008.

[9] Amit Deshpande, Peter Sicinski, and Philip W. Hinds. Cyclins and cdks in development and cancer: a perspective. *Oncogene*, 24(17):2909–2915, 2005.

[10] J. M. Adams and S. Cory. The bcl-2 apoptotic switch in cancer development and therapy. *Oncogene*, 26(9):1324–1337, 2007.

[11] Melissa R. Junttila and Gerard I. Evan. p53 — a jack of all trades but master of none. *Nature Reviews Cancer*, 9(11):821–829, November 2009.

[12] Scott W. Lowe, Enrique Cepero, and Gerard Evan. Intrinsic tumour suppression. *Nature*, 432(7015):307–315, November 2004.

[13] Steven E. Artandi and Ronald A. DePinho. Telomeres and telomerase in cancer. *Carcinogenesis*, 31(1):9–18, January 2010.

[14] Yusheng Cong and Jerry W. Shay. Actions of human telomerase beyond telomeres. *Cell Research*, 18(7):725–732, 2008.

[15] Douglas Hanahan. Patterns and emerging mechanisms of the angiogenic switch during tumorigenesis. *Cell*, 86:353–364, 1996.

[16] Napoleone Ferrara. Vascular endothelial growth factor. *Arteriosclerosis, Thrombosis, and Vascular Biology*, 29(6):789–791, June 2009.

[17] Kai Kessenbrock, Vicki Plaks, and Zena Werb. Matrix metalloproteinases: Regulators of the tumor microenvironment. *Cell*, 141(1):52–67, April 2010.

[18] Michael W. Klymkowsky and Pierre Savagner. Epithelial-mesenchymal transition. *The American Journal of Pathology*, 174(5):1588–1593, May 2009.

[19] Kornelia Polyak, Izhak Haviv, and Ian G. Campbell. Co-evolution of tumor cells and their microenvironment. *Trends in Genetics*, 25(1):30–38, January 2009.

[20] Jean Paul Thiery, Hervé Acloque, Ruby Y.J. Huang, and M. Angela Nieto. Epithelial-mesenchymal transitions in development and disease. *Cell*, 139(5):871–890, November 2009.

[21] Geert Berx and Frans van Roy. Involvement of members of the cadherin superfamily in cancer. *Cold Spring Harbor Perspectives in Biology*, 1(6), December 2009.

[22] Ugo Cavallaro and Gerhard Christofori. Cell adhesion and signalling by cadherins and ig-CAMs in cancer. *Nature Reviews Cancer*, 4(2):118–132, February 2004.

[23] Douglas Micalizzi, Susan Farabaugh, and Heide Ford. Epithelial-mesenchymal transition in cancer: Parallels between normal development and tumor progression. *Journal of Mammary Gland Biology and Neoplasia*, 15(2):117–134, 2010.

[24] Joseph H. Taube, Jason I. Herschkowitz, Kakajan Komurov, Alicia Y. Zhou, Supriya Gupta, Jing Yang, Kimberly Hartwell, Tamer T. Onder, Piyush B. Gupta, Kurt W. Evans, Brett G. Hollier, Prahlad T. Ram, Eric S. Lander, Jeffrey M. Rosen, Robert A. Weinberg, and Sendurai A. Mani. Core epithelial-to-mesenchymal transition interactome gene-expression signature is associated with claudin-low and metaplastic breast cancer subtypes. *Proceedings of the National Academy of Sciences*, 107(35):15449–15454, August 2010.

[25] Ilona N. Holcomb, Douglas I. Grove, Martin Kinnunen, Cynthia L. Friedman, Ian S. Gallaher, Todd M. Morgan, Cassandra L. Sather, Jeffrey J. Delrow, Peter S. Nelson, Paul H. Lange, William J. Ellis, Lawrence D. True, Janet M. Young, Li Hsu, Barbara J. Trask, and Robert L. Vessella. Genomic alterations indicate

tumor origin and varied metastatic potential of disseminated cells from prostate cancer patients. *Cancer Research*, 68(14):5599–5608, July 2008.

[26] Russell G. Jones and Craig B. Thompson. Tumor suppressors and cell metabolism: a recipe for cancer growth. *Genes & Development*, 23(5):537–548, March 2009.

[27] Li Yang, Yanli Pang, and Harold L. Moses. TGF-beta and immune cells: an important regulatory axis in the tumor microenvironment and progression. *Trends in Immunology*, 31(6):220–227, June 2010.

[28] Jacqueline D. Shields, Iraklis C. Kourtis, Alice A. Tomei, Joanna M. Roberts, and Melody A. Swartz. Induction of lymphoidlike stroma and immune escape by tumors that express the chemokine CCL21. *Science*, 328(5979):749–752, May 2010.

[29] Dimitrios Mougiakakos, Aniruddha Choudhury, Alvaro Lladser, Rolf Kiessling, and C. Christian Johansson. Chapter 3 - regulatory t cells in cancer. In George F. Vande Woude and George Klein, editors, *Advances in Cancer Research*, volume Volume 107, pages 57–117. Academic Press, 2010.

[30] Suzanne Ostrand-Rosenberg and Pratima Sinha. Myeloid-derived suppressor cells: Linking inflammation and cancer. *The Journal of Immunology*, 182(8):4499–4506, April 2009.

[31] Stanley Zucker, Jian Cao, and Wen-Tien Chen. Critical appraisal of the use of matrix metalloproteinase inhibitors in cancer treatment. *Oncogene*, 19(56):6642–6650, December 2000.

[32] Renea A. Taylor, Roxanne Toivanen, and Gail P. Risbridger. Stem cells in prostate cancer: treating the root of the problem. *Endocrine-Related Cancer*, 17(4):R273–R285, December 2010.

[33] Xi Wang, Marianna Kruithof-de Julio, Kyriakos D. Economides, David Walker, Hailong Yu, M. Vivienne Halili, Ya-Ping Hu, Sandy M. Price, Cory Abate-Shen, and Michael M. Shen. A luminal epithelial stem cell that is a cell of origin for prostate cancer. *Nature*, 461(7263):495–500, September 2009.

[34] Y. Wang, S. W. Hayward, M. Cao, K. A. Thayer, and G. R. Cunha. Cell differentiation lineage in the prostate. *Differentiation*, 68(4-5):270–279, 2001.

[35] Gavin D. Richardson, Craig N. Robson, Shona H. Lang, David E. Neal, Norman J. Maitland, and Anne T. Collins. CD133, a novel marker for human prostatic epithelial stem cells. *Journal of Cell Science*, 117(16):3539–3545, July 2004.

[36] Kevin G. Leong, Bu-Er Wang, Leisa Johnson, and Wei-Qiang Gao. Generation of a prostate from a single adult stem cell. *Nature*, 456(7223):804–808, October 2008.

[37] Devon A. Lawson, Li Xin, Rita U. Lukacs, Donghui Cheng, and Owen N. Witte. Isolation and functional characterization of murine prostate stem cells. *Proceedings of the National Academy of Sciences*, 104(1):181–186, January 2007.

[38] Andrew S. Goldstein, Devon A. Lawson, Donghui Cheng, Wenyi Sun, Isla P. Garraway, and Owen N. Witte. Trop2 identifies a subpopulation of murine and human prostate basal cells with stem cell characteristics. *Proceedings of the National Academy of Sciences*, 105(52):20882–20887, December 2008.

[39] Michael M. Shen and Cory Abate-Shen. Molecular genetics of prostate cancer: new prospects for old challenges. *Genes & Development*, 24(18):1967–2000, September 2010.

[40] Robert E. Reiter, Zhennen Gu, Tetsuro Watabe, George Thomas, Kinga Szigeti, Elizabeth Davis, Matthew Wahl, Sazuku Nisitani, Joyce Yamashiro, Michelle M. Le

Beau, Massimo Loda, and Owen N. Witte. Prostate stem cell antigen: A cell surface marker overexpressed in prostate cancer. *Proceedings of the National Academy of Sciences*, 95(4):1735–1740, February 1998.

[41] Berend Snijder, Raphael Sacher, Pauli Rämö, Eva-Maria Damm, Prisca Liberali, and Lucas Pelkmans. Population context determines cell-to-cell variability in endocytosis and virus infection. *Nature*, 461(7263):520–523, August 2009.

[42] Arjun Raj and Alexander van Oudenaarden. Nature, nurture, or chance: Stochastic gene expression and its consequences. *Cell*, 135(2):216–226, October 2008.

[43] Narendra Maheshri and Erin K. O'Shea. Living with noisy genes: How cells function reliably with inherent variability in gene expression. *Annual Review of Biophysics and Biomolecular Structure*, 36(1):413–434, 2007.

[44] Michael B. Elowitz, Arnold J. Levine, Eric D. Siggia, and Peter S. Swain. Stochastic gene expression in a single cell. *Science*, 297(5584):1183–1186, August 2002.

[45] Berend Snijder and Lucas Pelkmans. Origins of regulated cell-to-cell variability. *Nature Reviews Molecular Cell Biology*, 12(2):119–125, February 2011.

[46] Steven A Sundberg. High-throughput and ultra-high-throughput screening: solution- and cell-based approaches. *Current Opinion in Biotechnology*, 11(1):47–53, February 2000.

[47] A. M. Maffia III, I. Kariv, and K. R. Oldenburg. Miniaturization of a mammalian cell-based assay: luciferase reporter gene readout in a 3 microliter 1536-well plate. *Journal of biomolecular screening*, 4(3):137–142, 1999.

[48] K. R. Oldenburg, J. H. Zhang, T. Chen, A. Maffia, K. F. Blom, A. P. Combs, and T. D. Y. Chung. Assay miniaturization for ultra-high throughput screening of

combinatorial and discrete compound libraries: A 9600-well (0.2 microliter) assay system. *Journal of Biomolecular Screening*, 3(1):55–62, 1998.

[49] Jenifer Clausell-Tormos, Diana Lieber, Jean-Christophe Baret, Abdeslam El-Harrak, Oliver J. Miller, Lucas Frenz, Joshua Blouwolff, Katherine J. Humphry, Sarah Köster, Honey Duan, Christian Holtze, David A. Weitz, Andrew D. Griffiths, and Christoph A. Merten. Droplet-based microfluidic platforms for the encapsulation and screening of mammalian cells and multicellular organisms. *Chemistry & Biology*, 15(5):427–437, May 2008.

[50] S. Y. Teh, R. Lin, L. H. Hung, and A. P. Lee. Droplet microfluidics. *Lab Chip*, 8(2):198–220, 2008.

[51] Petra S. Dittrich and Andreas Manz. Lab-on-a-chip: microfluidics in drug discovery. *Nature Reviews Drug Discovery*, 5(3):210–218, March 2006.

[52] L. D. Landau. Fluid mechanics: Volume 6 (Course of theoretical physics) author: LD landau, EM lifshitz, publisher: Bu. 1987.

[53] Martin U. Kopp, Andrew J. de Mello, and Andreas Manz. Chemical amplification: Continuous-flow PCR on a chip. *Science*, 280(5366):1046–1048, May 1998.

[54] Andrew G. Ewing, Peter F. Gavin, Paula Beyer Hietpas, and Katherine M. Bullard. Continuous separations in microfabricated channels for monitoring ultrasmall biological environments. *Nature Medicine*, 3(1):97–99, January 1997.

[55] S. Takayama, E. Ostuni, P. LeDuc, K. Naruse, D. E. Ingber, G. M. Whitesides, et al. Subcellular positioning of small molecules. *Nature*, 411(6841):1016, 2001.

[56] R. J. Taylor, D. Falconnet, A. Niemistö, S. A. Ramsey, S. Prinz, I. Shmulevich, T. Galitski, and C. L. Hansen. Dynamic analysis of MAPK signaling using a high-

throughput microfluidic single-cell imaging platform. *Proceedings of the National Academy of Sciences*, 106(10):3758–3763, March 2009.

[57] Elena M. Lucchetta, Ji Hwan Lee, Lydia A. Fu, Nipam H. Patel, and Rustem F. Ismagilov. Dynamics of drosophila embryonic patterning network perturbed in space and time using microfluidics. *Nature*, 434(7037):1134–1138, April 2005.

[58] Matthew R. Bennett, Wyming Lee Pang, Natalie A. Ostroff, Bridget L. Baumgartner, Sujata Nayak, Lev S. Tsimring, and Jeff Hasty. Metabolic gene regulation in a dynamically changing environment. *Nature*, 454(7208):1119–1122, July 2008.

[59] Yuichi Taniguchi, Paul J. Choi, Gene-Wei Li, Huiyi Chen, Mohan Babu, Jeremy Hearn, Andrew Emili, and X. Sunney Xie. Quantifying e. coli proteome and transcriptome with single-molecule sensitivity in single cells. *Science*, 329(5991):533–538, July 2010.

[60] Siew-Min Ong, Chi Zhang, Yi-Chin Toh, So Hyun Kim, Hsien Loong Foo, Choon Hong Tan, Danny van Noort, Sungsu Park, and Hanry Yu. A gel-free 3D microfluidic cell culture system. *Biomaterials*, 29(22):3237–3244, August 2008.

[61] N. Chronis, M. Zimmer, and C. I. Bargmann. Microfluidics for in vivo imaging of neuronal and behavioral activity in caenorhabditis elegans. *Nature methods*, 4(9):727–731, 2007.

[62] Nannan Ye, Jianhua Qin, Weiwei Shi, Xin Liu, and Bingcheng Lin. Cell-based high content screening using an integrated microfluidic device. *Lab on a Chip*, 7(12):1696, 2007.

[63] Savaş Tay, Jacob J. Hughey, Timothy K. Lee, Tomasz Lipniacki, Stephen R. Quake, and Markus W. Covert. Single-cell NF-kappaB dynamics reveal digital activation and analogue information processing. *Nature*, 466(7303):267–271, July 2010.

[64] Laurence R. Brewer and Piero R. Bianco. Laminar flow cells for single-molecule studies of DNA-protein interactions. *Nature Methods*, 5(6):517–525, June 2008.

[65] Tomer Kalisky and Stephen R. Quake. Single-cell genomics. *Nature Methods*, 8(4):311–314, 2011.

[66] Jianbin Wang, H. Christina Fan, Barry Behr, and Stephen R. Quake. Genome-wide single-cell analysis of recombination activity and de novo mutation rates in human sperm. *Cell*, 150(2):402–412, July 2012.

[67] Bachir El Debs, Ramesh Utharala, Irina V. Balyasnikova, Andrew D. Griffiths, and Christoph A. Merten. Functional single-cell hybridoma screening using droplet-based microfluidics. *Proceedings of the National Academy of Sciences*, 109(29):11570–11575, July 2012.

[68] Paul H. Bessette, Xiaoyuan Hu, Hyongsok T. Soh, and Patrick S. Daugherty. Microfluidic library screening for mapping antibody epitopes. *Analytical Chemistry*, 79(5):2174–2178, March 2007.

[69] Wei Wang, Chun Yang, YingShuai Liu, and Chang Ming Li. On-demand droplet release for droplet-based microfluidic system. *Lab on a Chip*, 10(5):559, 2010.

[70] Ali Fallah-Araghi, Jean-Christophe Baret, Michael Ryckelynck, and Andrew D. Griffiths. A completely in vitro ultrahigh-throughput droplet-based microfluidic screening system for protein engineering and directed evolution. *Lab on a Chip*, 12(5):882, 2012.

[71] Jeremy J. Agresti, Eugene Antipov, Adam R. Abate, Keunho Ahn, Amy C. Rowat, Jean-Christophe Baret, Manuel Marquez, Alexander M. Klibanov, Andrew D. Griffiths, and David A. Weitz. Ultrahigh-throughput screening in drop-based micro-

fluidics for directed evolution. *Proceedings of the National Academy of Sciences*, 107(9):4004–4009, March 2010.

[72] Dominic Eicher and Christoph A Merten. Microfluidic devices for diagnostic applications. *Expert Review of Molecular Diagnostics*, 11(5):505–519, June 2011.

[73] Jenifer Clausell-Tormos. Development of a two-phase microfluidic platform for drug screening. *PhD manuscript*, 2010.

[74] C. Holtze, A. C. Rowat, J. J. Agresti, J. B. Hutchison, F. E. Angile, C. H. J. Schmitz, S. Köster, H. Duan, K. J. Humphry, R. A. Scanga, et al. Biocompatible surfactants for water-in-fluorocarbon emulsions. *Lab Chip*, 8(10):1632–1639, 2008.

[75] Huaping Xiao, Dan Guo, Shuhai Liu, Guoxin Xie, Guoshun Pan, Xinchun Lu, and Jianbin Luo. Direct observation of oil displacement by water flowing toward an oil nanogap. *Journal of Applied Physics*, 110(4):044906 –044906–4, August 2011.

[76] J. C. Baret, O. J. Miller, V. Taly, M. Ryckelynck, A. El-Harrak, L. Frenz, C. Rick, M. L. Samuels, J. B. Hutchison, J. J. Agresti, et al. Fluorescence-activated droplet sorting (FADS): efficient microfluidic cell sorting based on enzymatic activity. *Lab Chip*, 9(13):1850–1858, 2009.

[77] Jean-louis Viovy and Max Chabert. Encapsulation microfluidic device, November 2011. Patent number 20110285042 and application number 13/120310, issued on 11/24/2011.

[78] Evelien W. M. Kemna, Rogier M. Schoeman, Floor Wolbers, Istvan Vermes, David A. Weitz, and Albert van den Berg. High-yield cell ordering and deterministic cell-in-droplet encapsulation using dean flow in a curved microchannel. *Lab on a Chip*, 2012.

[79] Bachir El Debs. Functional single-cell hybridoma screening using droplet-based microfluidics. *PhD manuscript*, 2011.

[80] Peter Mitchell. Microfluidics—downsizing large-scale biology. *Nature Biotechnology*, 19(8):717–721, 2001.

[81] Saleema Saleh-Lakha and Jack T. Trevors. Perspective: Microfluidic applications in microbiology. *Journal of Microbiological Methods*, 82(1):108–111, July 2010.

[82] Malene S. Thomsen, Peter Polt, and Bernd Nidetzky. Development of a microfluidic immobilised enzyme reactor. *Chemical Communications*, (24):2527, 2007.

[83] Hanbin Mao, Tinglu Yang, and Paul S. Cremer. Design and characterization of immobilized enzymes in microfluidic systems. *Analytical Chemistry*, 74(2):379–385, January 2002.

[84] Pedro Fernandes. Miniaturization in biocatalysis. *International Journal of Molecular Sciences*, 11(3):858–879, March 2010.

[85] Masaya Miyazaki and Hideaki Maeda. Microchannel enzyme reactors and their applications for processing. *Trends in Biotechnology*, 24(10):463–470, October 2006.

[86] B. P. Mason, K. E. Price, J. L. Steinbacher, A. R. Bogdan, and D. T. McQuade. Greener approaches to organic synthesis using microreactor technology. *ChemInform*, 38(36):no–no, 2007.

[87] M. Tisma, B. Zelić, D.J. Vasić-Racki, P. Znidarsic-Plazl, and I. Plazl. Modelling of laccase-catalyzed l-DOPA oxidation in a microreactor. *Chemical Engineering Journal*, 149(1):383–388, 2009.

[88] K. Kanno, H. Maeda, S. Izumo, M. Ikuno, K. Takeshita, A. Tashiro, and M. Fujii. Rapid enzymatic transglycosylation and oligosaccharide synthesis in a microchip reactor. *Lab Chip*, 2(1):15–18, 2002.

[89] Ping He, Gillian Greenway, and Stephen Haswell. Development of enzyme immobilized monolith micro-reactors integrated with microfluidic electrochemical cell for the evaluation of enzyme kinetics. *Microfluidics and Nanofluidics*, 8(5):565–573, 2010.

[90] Alexandra Schwarz, Malene S. Thomsen, and Bernd Nidetzky. Enzymatic synthesis of beta-glucosylglycerol using a continuous-flow microreactor containing thermostable beta-glycoside hydrolase CelB immobilized on coated microchannel walls. *Biotechnology and Bioengineering*, 103(5):865–872, 2009.

[91] Christopher J. Cullen, Robert C. R. Wootton, and Andrew J. de Mello. Microfluidic systems for high-throughput and combinatorial chemistry. *ChemInform*, 36(27):no–no, 2005.

[92] Paul Watts and Stephen J Haswell. Microfluidic combinatorial chemistry. *Current Opinion in Chemical Biology*, 7(3):380–387, June 2003.

[93] Enrico Mastrobattista, Valerie Taly, Estelle Chanudet, Patrick Treacy, Bernard T. Kelly, and Andrew D. Griffiths. High-throughput screening of enzyme libraries: In vitro evolution of a beta-galactosidase by fluorescence-activated sorting of double emulsions. *Chemistry & Biology*, 12(12):1291–1300, December 2005.

Appendix

List of Figures

List of Tables